HHS Public Access

Author manuscript

Cell Metab. Author manuscript; available in PMC 2025 January 02.

Published in final edited form as:

Cell Metab. 2024 January 02; 36(1): 90–102.e7. doi:10.1016/j.cmet.2023.11.018.

Repression of Latent NF-κB Enhancers by PDX1 Regulates β-cell Functional Heterogeneity

Benjamin J. Weidemann[1], **Biliana Marcheva**[1], **Mikoto Kobayashi**[1], **Chiaki Omura**[1], **Marsha V. Newman**[1], **Yumiko Kobayashi**[1], **Nathan J. Waldeck**[1], **Mark Perelis**[1,2], **Louise Lantier**[3,4], **Owen P. McGuinness**[3,4], **Kathryn Moynihan Ramsey**[1], **Roland W. Stein**[4], **Joseph Bass**[1,*]

[1]Department of Medicine, Division of Endocrinology, Metabolism and Molecular Medicine, Northwestern University Feinberg School of Medicine, Chicago, IL, 60611, USA.

[2]Ionis Pharmaceuticals, Carlsbad, CA, 92010, USA.

[3]Vanderbilt-NIH Mouse Metabolic Phenotyping Center, Nashville, TN, 37232, USA.

[4]Department of Molecular Physiology and Biophysics, Vanderbilt University Medical Center, Nashville, TN, 37232, USA.

SUMMARY

Interactions between lineage-determining and activity-dependent transcription factors determine single-cell identity and function within multicellular tissues through incompletely known mechanisms. By assembling a single-cell atlas of chromatin state within human islets, we identified β-cell subtypes governed by either high or low activity of the lineage-determining factor pancreatic duodenal homeobox-1 (PDX1). β cells with reduced PDX1 activity displayed increased chromatin accessibility at latent NF-κB enhancers. *Pdx1* hypomorphic mice exhibited de-repression of NF-κB and impaired glucose tolerance at night. Three-dimensional analyses in tandem with ChIP-sequencing revealed that PDX1 silences NF-κB at circadian and inflammatory enhancers through long-range chromatin contacts involving SIN3A. Conversely, *Bmal1* ablation in β cells disrupted genome-wide PDX1 and NF-κB DNA binding. Finally, antagonizing the IL-1β receptor, an NF-κB target, improved insulin secretion in *Pdx1* hypomorphic islets. Our studies reveal functional subtypes of single β cells defined by a gradient in PDX1 levels and identify NF-κB as a target for insulinotropic therapy.

[*]**Corresponding Author and Lead Contact:** Joseph Bass, M.D., Ph.D., Department of Medicine, Feinberg School of Medicine, Division of Endocrinology, Metabolism and Molecular Medicine, 303 East Superior Street Lurie 7-107, Chicago, Illinois 60611, Phone: 312-503-2258, Fax: 312-503-5453, j-bass@northwestern.edu.

AUTHOR CONTRIBUTIONS

B.J.W. and J.B. conceived and designed the studies. B.J.W., B.M., M.K., C.O., M.V.N, Y.K., L.L., and O.P.M performed experiments. N.J.W. and M.P. helped with analyses. R.W.S. provided the *Pdx1* mutant mice. B.J.W., K.M.R., and J.B. wrote the manuscript. All authors discussed the results and commented on the manuscript.

DECLARATION OF INTERESTS

B.J.W., B.M., M.K., C.O., M.V.N., Y.K., N.J.W., L.L., O.P.M., K.M.R., R.W.S., and J.B. declare no competing interests. M.P. is currently affiliated with Ionis Pharmaceuticals, Inc but has no financial interests to declare.

Graphical Abstract

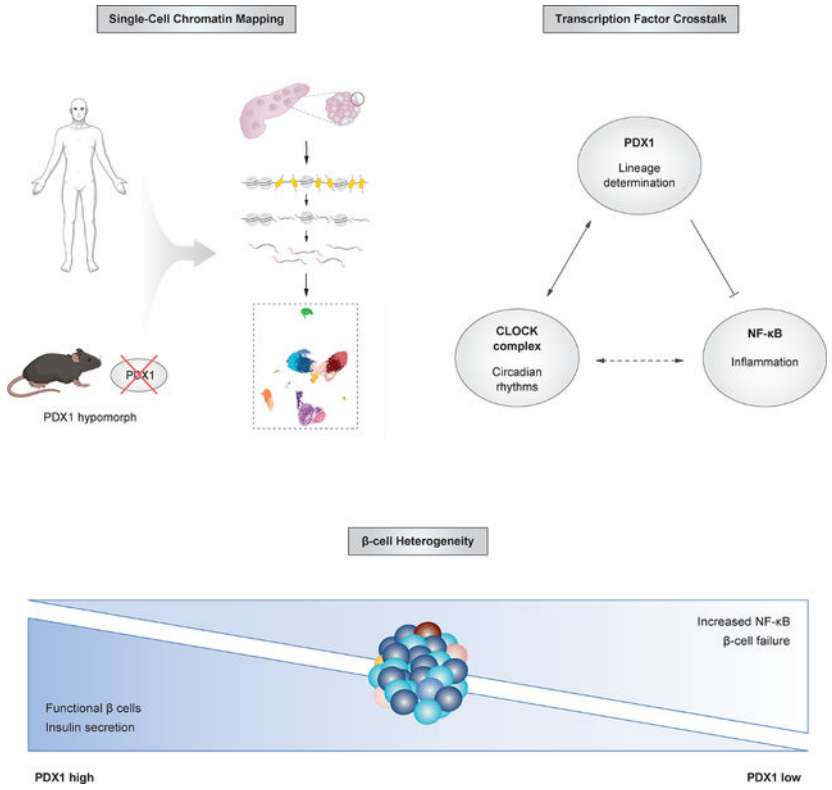

eTOC BLURB

Transcription factor dynamics within individual cells drive β-cell identity and function. Weidemann *et al.* employ single-cell analyses within human and murine models to reveal reciprocal regulation of PDX1 and NF-κB by the clock in distinct β-cell sub-populations and provide logic for anti-inflammatory therapy to reverse β-cell failure caused by PDX1 deficiency.

Keywords

NF-κB; p65; circadian; PDX1; SIN3A; islets; insulin; inflammation; single-cell ATAC-sequencing; IL-1β; diabetes

INTRODUCTION

Collaboration between lineage-determining and signal-dependent transcription factors (LDTFs and SDTFs) sustains energy constancy in response to changes in the nutrient environment associated with the fasting-feeding cycle[1,2]. The circadian clock also orchestrates anticipatory cycles of transcription within nearly all metabolic tissues, yet how circadian, nutrient, and lineage-dependent pathways interact within individual cells of multicellular tissues remains unknown[3–7].

The endocrine pancreas is a heterogenous organ that exhibits pronounced oscillation in function across the light-dark cycle and is composed of distinct glucoregulatory cell types. Identity of insulin-producing β-cells is initiated during the primary transition from the pancreatic endodermal bud through combinatorial interactions between pancreatic duodenal homeobox factor 1 (PDX1) and the NK6 homeodomain factor NKX6.1, the basic leucine-zipper MAFA, and hepatocyte nuclear factors (HNFs)[2,8,9]. PDX1 also promotes β-cell ontogeny through repression of α-cell gene networks including those controlled by aristaless-related homeobox (ARX)[6,10] and repression of factors that impair aerobic metabolism such as the carboxylate-transporter(s)[11,12]. Following weaning, PDX1 induces the expression of genes important in glucose-stimulated insulin secretion that are co-regulated by the core clock transcription factors CLOCK and BMAL1[7]. BMAL1 has also been shown to stabilize β-cell identity by preventing α-cell gene expression during regeneration in response to diptheria-induced cell damage[13]. A remaining question is whether impaired function of LDTFs may contribute to β cell failure in adulthood[14–18].

Here we use epigenomic analyses to identify and dissect the crosstalk between lineage- and signal-dependent transcriptional networks within human and murine islets. We identify distinct subtypes of β cells characterized by differences in the activity of the lineage factor PDX1, in addition to variation in the activity of both inflammatory and circadian gene networks. Our studies reveal that β cells with high PDX1 activity exhibit accessibility at gene networks involved in insulin secretion that are also controlled by the molecular clock. In contrast, β cells with low PDX1 activity exhibit greater chromatin accessibility within enhancers of NF-κB-induced genes. We also show that treatment of islets from *Pdx1* hypomorphic animals with an IL-1β receptor blocking peptide enhances insulin secretory capacity. Our studies reveal that loss of PDX1-mediated repression of latent NF-κB enhancers leads to β-cell failure and provide rationale for targeting NF-κB to treat hypoin-sulinemia.

RESULTS

Single-cell chromatin accessibility sequencing identifies PDX1 and latent NF-κB enhancer signatures within distinct β-cell populations of the human islet

Pancreatic islets consist of diverse cell populations that produce physiologically-opposing hormones important in fasting and postprandial glucose metabolism. Recent single-cell sequencing analyses have suggested that within the islet, insulin-producing cells exhibit heterogeneity based upon distinct patterns of accessibility within cis-regulatory elements (CREs)[3,14,19]. CREs that identify putative β-cell subtypes also encompass noncoding variants linked to risk of type 2 diabetes[20,21]. To elucidate how combinatorial interactions between lineage- and signal-dependent transcription factors might determine β-cell heterogeneity and function, we profiled chromatin accessibility and TF binding motifs in human cadaveric islets obtained from the Integrated Islet Distribution Program (IIDP) using single-nuclei assay of transposase accessible chromatin-sequencing (snATAC-seq) (Figure 1A). We identified 334,116 accessible CREs across 20,519 single islet cells, which were grouped into 19 distinct clusters using the Uniform Manifold Approximation and Projection (UMAP) dimensional reduction approach (see STAR Methods). These 19 clusters included

canonical endocrine cell types, with four α cell clusters (α1–4), three β cell clusters (β1–3), and one δ cell cluster (Figure 1B), which were characterized by chromatin accessibility nearby genes encoding glucagon (*GCG*), insulin/insulin-like growth factor 2 (*INS/IGF2*), and somatostatin (*SST*), respectively (Figure 1C). Other islet-associated cell subpopulations identified by accessibility at canonical cell markers included stellate (*PDGFRB*), neural crest (*SOX10*), lymphatic and myeloid immune (*CCL4*), endothelial (*PECAM1*), ductal (*KRT19*), and acinar (*REG1A*) cells (Figures 1B–C).

A key advantage of snATAC-seq over single-cell mRNA transcriptomic profiling lies in the ability to detect the regulatory activity of TFs at both gene promoters and distal enhancers[19,22–24]. To examine whether differential gene regulation underlies β-cell heterogeneity, we first compared gene activity scores (the sum of accessible reads at fragments overlapping gene coordinates and the 2 kb region upstream) between the β1 and β2 β-cell subclusters, which comprised 47.2 and 45.1% of the total β-cell population, respectively. We identified 600 genes with significant variation ($P < 0.05$), including β-cell-defining genes such as *INS* (6.45e-87), *MAFA* (2.25e-50), and *GLP1R* (2.37e-36), and inflammatory genes such as *PTGER3* (1.471551e-05), *IL2* (5.968259e-15), and *LPAR1* (8.646495e-15) (Figure S1A) (Table S1). Analysis of single-cell RNA-sequencing (scRNA-seq) from 12 non-diabetic human islets (GSE114297), using snATAC-seq gene activity scores as transfer anchors for clustering within Seurat, revealed significant correlation between $\log_2$-fold changes in RNA expression and chromatin gene activity scores between the β1 and β2 subpopulations ($P = 1.29e-30$, Pearson's $r = 0.35$) (Figure S1B). A similar correspondence between changes in gene expression and chromatin accessibility was observed when comparing α cell sub-populations (Table S2) and when comparing whole α and β cell populations directly ($P = 1.0e-16$, Pearson's $r = 0.75$) (Figure S1B). These data reveal correspondence between single-cell transcript abundance and chromatin accessibility across cell types[25].

To elucidate the epigenetic mechanisms underlying β-cell heterogeneity, we compared differential CREs between the *INS*-enriched (β1) and *INS*-low (β2) β-cell clusters (Figures S1A, S1C) and found that the majority of differentially-accessible sites (73.29% of 2,632 peaks) were located within enhancer regions (either greater than 3 kb upstream or 1 kb downstream of transcription start sites) ($P_{adj} < 0.05$) (Figure S1D). We next took advantage of our robust sequencing depth per cell (37,400 high-quality fragments per cell) to identify differential TF activity in the β1 versus β2 subpopulations using chromVAR to measure TF-associated chromatin accessibility[26, 27]. Comparison of motif Z-scores between the β1 and β2 cell clusters identified differential accessibility at several β-cell lineage-determining transcription factor (LDTF) motifs that corresponded with increased accessibility nearby *INS* (Figures 1D, S1A). Among the established LDTFs, PDX1, a master regulator of pancreatic development[28], was one of the most significant differentially-enriched motifs (Padj=3.98e-88) that was also one of the most highly expressed TFs within adult β cells (Figures 1D–E, S1E). We further found that 58% of the differentially-accessible sites between β1 and β2 cells contained motifs for PDX1 compared to 40% in the background peak set (hypergeometric test, $P < 0.001$) (Figure S1D). We therefore refer to these β1 and β2 subpopulations as $PDX1^{high}$ and $PDX1^{low}$ cells, respectively. Other TFs that were enriched in the $PDX1^{high}$ cells were ones known to be required for mature β-cell

development, including neurogenic differentiation 1 (NEUROD1), NKX6.1, and the basic helix loop helix (bHLH) pancreas transcription factor 1A (PTF1A), as well as other basic helix-loop-helix (bHLH) TFs whose DNA-binding motif contains canonical E-box motifs that are targets of the molecular clock[29,30] ($P_{adj} < 0.001$) (Figure 1E) (Table S3). In contrast, the subcluster of β2 cells with low accessibility at the *INS* locus was highly enriched for accessible nuclear factor-kappa B1 (NF-κB1), the kruppel-like factor KLF14, JUNB, and the interferon regulatory factor-6 (IRF6) TF motifs ($P_{adj} < 0.001$) (Figure 1E) (Table S3), all of which function in signal-induced expression of inflammatory genes during stress, the immune response, and in cell proliferation and survival[31,32]. These data support recent snATAC-seq studies that identified divergent hormone-high and hormone-low endocrine islet subtypes with unique immediate-early TF signatures[3,26] (GSE160472, GSE160473, GSE163610). We note a key advantage of our studies was the use of live tissue with the 10X Genomics platform[33], which enabled ~10-fold deeper sequencing read coverage per cell than prior studies and detection of rarer chromatin opening events including at NF-κB sites. In sum, our single-cell sequencing of chromatin activity identified bimodal populations of insulin-producing cells within the human islet – one *INS*-enriched cluster with high PDX1 activity and one *INS*-low cluster with low PDX1 activity but with significant enrichment in NF-κB TF activity. We also examined *PDX1* RNA abundance in human islets using RNAscope, which revealed a bimodal distribution of *PDX1* RNA levels in contrast to the normal distribution observed in various housekeeping genes (Figure S1F). These observations support the existence of two distinct populations of β cells with respect to PDX1 activity.

Collaborative interactions amongst TFs define individual subpopulations of the mature β cell, and our data suggests that known regulators of β-cell maturation and function are uniquely activated in $PDX1^{high}$ β cells[34–36]. The circadian clock activators CLOCK/BMAL1 have been shown to contribute to metabolic maturation and identity of insulin-producing cells, through the underlying mechanisms remain poorly understood[37,38]. The findings above that PDX1 and clock regulatory elements co-exist in *INS*-enriched clusters support the possibility that PDX1 and rhythmic gene expression may play a role in β-cell function. To examine whether transcriptional regulators of β-cell identity are regulated in a circadian manner, we assessed 24-hr rhythmic opening of chromatin by performing ATAC-seq in human islets whose molecular clocks were first synchronized using a 1-hr forskolin pulse. Genomic analyses were performed every 4 hrs for 24 hrs starting >24 hrs after administration of forskolin, well beyond the ~1-hr half-life of forskolin action on chromatin[39] (Figure 1A). We generated within-donor z-scores across the 24-hr times series using normalized ATAC-seq counts (see STAR Methods) and identified 3,125 statistically rhythmic ATAC-seq peaks genome-wide using the empirical Jonckheere-Terpstra-Kendall algorithm (eJTK_CYCLE) (Bonferroni $P < 0.05$) (Figure 1F)[40]. Rhythmic sites were identified near enhancers of genes implicated in islet cell identity (*SIX3*, *PDX1*, *GCG*), circadian expression (*PER2*, *NPAS2*), and inflammation (*ETS2*, *TNFRSF21*)[41–43]. TF motif enrichment analysis at rhythmic ATAC-seq peaks identified significant enrichment for TFs (e.g., PDX1, NEUROD1, and PTF1A) ($P_{adj} < 0.05$) (Figure 1F) that were also enriched in $PDX1^{high}$ cells (Figure 1E). Together, these studies indicate that rhythmic co-activation of chromatin by PDX1 and other TFs across the day may contribute to β-cell function.

PDX1 represses NF-κB enhancers to control β-cell function

Cross-talk between lineage and signal-dependent TFs within non-coding regulatory regions of the genome drive identity and function of the endocrine pancreas[24,44–46]. Emerging studies suggest that LDTFs define distinct subpopulations of β cells important in both insulin secretion and type 2 diabetes[3,15]. Based upon our finding of a PDX1 activity signature in distinct cell populations exhibiting divergent patterns of NF-κB and clock activity, we sought to dissect the function of PDX1 in control of inflammatory and circadian gene networks using snATAC-seq analyses of single-nuclei isolated from islets of mice with genetic deficiency of PDX1 (Figure 2A). Since ablation of *Pdx1* causes embryonic lethality, we utilized mice heterozygous for a null allele of *Pdx1* (*Pdx1*$^{+/-}$) in the presence or absence of second allele harboring a mutation within a key regulatory enhancer (area IV) of *Pdx1* (mutant *Pdx1*$^{\Delta IV/-}$ vs control *Pdx1*$^{+/-}$ mice, respectively) (Figure 2A). *Pdx1*$^{\Delta IV/-}$ mice develop post-weaning hypoinsulinemia, impaired glucose tolerance, and decreased β-cell proliferation[12,47]. Using merged snATAC-seq data derived from nuclei harvested post-weaning (10–18 weeks of age) from *Pdx1*$^{\Delta AIV/-}$ and control *Pdx1*$^{+/-}$ mice, we identified 187,343 accessible CREs from 9,480 single islet cells isolated and classified these into 15 unique islet cell populations, which included three β-cell populations (Figures 2B, S2A–C). These three murine β-cell populations varied according to PDX1 activity similar to our observations in human cadaveric islets (Figure 1B–E). Comparison of chromatin accessibility in the ensemble of all three β-cell populations of both *Pdx1*$^{\Delta AIV/-}$ mutant and *Pdx1*$^{+/-}$ genotypes revealed significant alterations in accessibility at 1,902 chromatin peaks across 1,373 unique genes ($P_{adj} < 0.05$). The *Pdx1* area IV enhancer region was the most significantly downregulated non-coding cis-regulatory element (Figure S2D), consistent with hemizygosity at this enhancer, followed by the *Ins1* promoter (Figure 2C) ($P < 0.001$). Motif analyses from the pooled β-cell populations revealed reduced chromatin accessibility in *Pdx1*$^{\Delta AIV/-}$ mutant mice at binding sites for key TFs that promote β-cell function, including NEUROD1, NEUROG2, PTF1A, and bHLH factors (Figure 2D), providing genetic evidence that supports our findings that in human islets, PDX1^{high} subpopulations correlated with TFs associated with β-cell and circadian function (Figures 1E–F). In contrast, sites that displayed increased chromatin accessibility in *Pdx1*-deficient mutants contained binding sites for TFs involved in proinflammatory signaling, including NF-κB1, NF-κB2, and RELA (Figure 2D). The finding of an altered chromatin landscape in islets from *Pdx1* hypomorphic animals with increased pro-inflammatory and reduced insulin secretory networks was analogous to our observation of unique enhancer signatures in human islets that were enriched or depleted in PDX1 and NF-κB, respectively (Figures 1E–F). Gene ontology pathway analysis further indicated a role for PDX1 in the induction of genes underlying glucose responsive insulin secretion in the β cell while at the same time repressing pro-inflammatory regulatory elements (Figure 2E). Peaks near closed chromatin in *Pdx1*$^{\Delta AIV/-}$ mutant β cells (i.e., increased accessibility in controls) were linked to pathways involved in hormone exocytosis, including MODY (e.g. *Iapp*, *Ins1*, *Pdx1*, *Mafa*) and type 2 diabetes mellitus (e.g. *Irs1*, *Mapk10*, *Mtor*, *Pparg*), as well as negative regulation of the acute inflammatory response (Figure 2E). In contrast, gene sets near chromatin that was more accessible in the mutant β cells were enriched within morphogenesis (e.g. *Egfr*, *Igf1r, Mapt*), negative regulation of synaptic transmission (e.g. *Asic1*, *Mgll*, *Pla2g6*, *Gabrb3*), and gene networks de-repressed following inhibition of the

circadian clock (e.g., *Bhlhe40*, *Ptger3*, *Cipc*) (Figure 2E)[48, 49]. However, we did not detect significant alterations in accessibility at cell-defining genes *Gcg* or *Sst* comparing α, β, or δ cells between *Pdx1* mutant and control endocrine cell populations (Figure S2E). Finally, RNA-sequencing revealed significantly reduced expression of genes involved in glucose-stimulated insulin secretion, including *Vamp2*, *Glp1r,* and *Snap25*, as well as those involved in circadian rhythms, including the *Per* and *Cry* genes, in islets isolated from $Pdx1^{\Delta AIV/-}$ mutant compared to control mice (Figure 2F), consistent with impaired β-cell function and disrupted circadian rhythms in $Pdx1^{\Delta AIV/-}$ mutants. Furthermore, we observed a significant enrichment and upregulation of genes involved in pro-inflammatory NF-κB-signaling and apoptosis (Figure 2F), supporting the de-repression of NF-κB signaling in the absence of PDX1. Therefore, studies in both *Pdx1* hypomorphic mice and in human islets indicate that PDX1 establishes a balance between the expression of circadian regulatory programs and NF-κB-mediated inflammatory pathways within the pancreatic β cells.

Circadian analyses reveal rhythmic regulation of NF-κB enhancer activity by PDX1

Circadian rhythms are first established within the β cell postnatally[50] and become more pronounced following weaning, where both a mixed macronutrient diet and induction of rhythmic feeding cycles lead to functional maturation of the β cell[51–53]. In the adult β cell, robust circadian clock activity promotes rhythmic insulin release through activation of pre-established enhancers that colocalize with PDX1 binding sites[2,7,51,54]. The observation that islets from *Pdx1*-deficient animals display compact chromatin within enhancers bound by circadian TFs (Figure 2E) prompted us to examine the effect of *Pdx1*-deficiency on the temporal regulation of β-cell enhancers. To examine chromatin accessibility in $Pdx1^{\Delta AIV/-}$ mutant and $Pdx1^{+/-}$ control islets at two different phases of the intrinsic circadian cycle, we exposed islets (n=3 biologically-independent pools of islets per genotype) to a 1-hr forskolin pulse and collected the islets at the nadir (36 hr time post-synchronization, TPS) and zenith (48 hr TPS) of rhythmic insulin secretion (Figure 3A)[7]. We performed ATAC-seq adapted for low-input samples following the Omni-ATAC-seq protocol[55] and identified 132,195 unique accessible sites across all pooled samples (Figure 3A). Likelihood ratio tests (LRTs) identified 1,207 significantly ($P_{adj} < 0.05$) altered CREs (Figures 3B–C) with respect to either circadian time or the *Pdx1* genotype using normalized ATAC-seq count data in DESeq2[56,57]. Unbiased principal component analysis using ATAC-seq normalized counts at these sites revealed distinct patterns of chromatin opening with respect to genotype and circadian time (Figure S3A).

To identify chromatin accessibility regulatory patterns among these data, we performed k-means clustering and identified three distinct clusters of genes that were dependent upon either circadian time and/or genotype. Group 1 sites had reduced accessibility at both time points in the *Pdx1* mutant islets but exhibited more robust opening at CT48 in the control islets, while group 2 sites gained accessibility specifically at CT36 and were more accessible in the *Pdx1* mutant islets (Figures 3B–C). Group 3 sites were regulated only by circadian time and not genotype (Figure S3C–D). Consistent with a collaborative role for the clock and PDX1 in promoting insulin secretion, Group 1 sites were enriched for PDX1, MAFA, and NKX6.1 binding motifs, including canonical PDX1 CREs that promote *Ins1* and *Mafa* expression ($P_{adj} < 0.001$) (Figures 3B–C)[7]. In contrast, distinct ATAC-seq peaks within the

Group 2 peak set enriched in the *Pdx1*-deficient cells occurred at sites near the inflammation mediators *Tnfrsf11b, Nfkbiz, Il-1b,* and the E26 transformation-specific (ETS) factors *Etv1* and *Ets2* (Figures 3B–D) and were enriched in motifs for NF-κB, RELA, and the immediate early complex FOS::JUNB (Figure 3C). These findings suggest that the loss of *Pdx1* results in both the de-repression and rhythmic reprogramming of inflammatory and stress response genes. Genes encoding the α-cell-enriched adrenergic receptors ADRB1 and ADRA1b in *Pdx1* mutant islets also exhibited increased circadian variation in accessibility, suggesting PDX1 normally represses islet α-cell transcription through mechanisms that may involve circadian factors (Figures 3B–F, S3B). Of note, lymphatic, macrophage, and exocrine cells in the $Pdx1^{\Delta AIV/-}$ mutants did not display differential PDX1 activity, indicating that increased chromatin accessibility of Group 2 genes could not be attributed to signal from non-β-cell types (Figure S2C). Finally, in contrast to Groups 1 and 2, which were dependent upon both genotype and circadian time, chromatin accessibility of Group 3 was only dependent upon circadian time (Figures 3B, S3C–D). These sites were enriched for DBP and NFIL3/E4BP4 TF motifs (Figure S3D), consistent with previous studies demonstrating that DBP regulates chromatin dynamics in the islet[58]. In sum, levels of PDX1 determine the chromatin landscape within subpopulations of the β cell characterized by unique patterns in the accessibility of enhancer regions controlling circadian and inflammatory gene programs.

To determine whether the divergent chromatin signatures identified in our synchronized ATAC-seq datasets correspond with diurnal insulin secretory dynamics in the whole animals, we performed oral glucose tolerance tests (oGTTs) in $Pdx1^{\Delta AIV/-}$ mutant and $Pdx1^{+/-}$ heterozygous control mice during both the day (ZT2) and night (ZT14). $Pdx1^{\Delta AIV/-}$ mutant mice displayed significantly impaired glucose tolerance compared to control mice ($P < 0.0001$) that was more pronounced during the nighttime (Figure 3E). Analysis of the whole glucose excursion curve by mixed effects modeling also revealed a significant interaction between the *Pdx1* genotype, time of day (i.e., zeitgeber time), and glucose levels ($P = 0.015$). These mice also had reduced insulin and C-peptide levels at both time points compared to controls ($P < 0.05$ by two-way ANOVA) (Figure 3E), and insulin and C-peptide levels were both reduced to a greater extent in the evening in the mutants relative to control animals[7]. Together, these data reveal a requirement for PDX1 in regulation of chromatin compaction, β-cell maturation, and glucose homeostasis across the day through alterations in the control of secretory and pro-inflammatory gene networks.

To examine whether the molecular clock contributes to rhythmic insulin secretion through the control of PDX1 chromatin binding, we performed PDX1 ChIP-seq in *Bmal1* knockout mouse β-cell lines (Beta-TC-6). We found that loss of BMAL1 led to significantly reduced PDX1 DNA binding genome wide within β cells ($P < 0.001$) (Figure S3F), including at regions controlling the expression of genes related to regulation of insulin secretion, including *Ins1*, *Neurod1*, and *Six2* (Figure S3F). Therefore, loss of the molecular clock leads to reciprocal impairment in PDX1-mediated regulation of genes important in β-cell function.

PDX1 forms long-range chromatin loops to regulate NF-κB and circadian clock enhancer activity

Given our observations that PDX1 and NF-κB regulatory elements distinguish distinct subpopulations of the adult β cell (Figures 1–2), we sought to determine whether PDX1 directly represses NF-κB genome-wide. We first examined how PDX1 depletion affects the activity of p65, a canonical NF-κB subunit, using p65 ChIP-seq in Beta-TC-6 treated for 48 hrs with siRNA targeting PDX1 compared to a control siRNA (Figure 4A). We observed that loss of PDX1 increased genome-wide occupancy of p65 at 5,268 unique sites, despite similar levels of p65 protein abundance (Figures 4A, S3E). This gain in binding included NF-κB/inflammation targets, such as *Tnfrs11a*, and the gene encoding the circadian repressor PER2 (Figure 4A), consistent with previous studies[59]. Luminometry analyses revealed that *Pdx1* hypomorphic islets exhibit a shortened period length (Figure S4A). Thus, loss of PDX1 in β cells increases NF-κB binding genome-wide and alters the expression of core clock repressors, suggesting that PDX1 repression of NF-κB in turn alters clock function.

Given our findings that ablation of *Bmal1* impaired PDX1 DNA binding (Figure S3F), we next sought to determine whether loss of the clock in turn alters the genome-wide binding of p65 by performing p65 ChIP-seq in *Bmal1* KO Beta-TC-6 cells. We observed significantly fewer p65 binding events in the *Bmal1* KO β cells (177 peaks) compared to controls (2430 peaks) (Figure S3G), suggesting BMAL1 is also required for the ability of p65 to bind chromatin. Sites depleted of p65 binding in the *Bmal1* KO cells included cell survival and anti-apoptotic genes, including the apoptosis antagonizing TF *Aatf*, janus kinase 1 *Jak1*, inositol polyphosphate-4-phosphatase *Inpp4b*, and the phosphodiesterase *Pde10a* (Figure S3G). This data suggests a three-way interaction in which activity of both PDX1 and p65 depends upon a functional circadian clock.

Three-dimensional chromatin analyses have revealed that LDTFs form contacts between widely-separated genomic regions to control β-cell function[15], yet whether PDX1 controls SDTFs through long-range contacts has not been determined (Figure 4B). Within *Pdx1*-knockdown β cells, p65 binding sites were enriched at positions far away (>500 bp) from sites of DNA binding by PDX1 observed in control cell types (Figure S4B). Therefore, we utilized three-dimensional chromosome conformation capture coupled with PDX1 ChIP-seq (HiChIP-seq) to map long-range interactions between PDX1 and distant regulatory elements (Figure 4B). We identified 4,155 long-range (> 5 kb) chromatin interactions between PDX1 and distant cis-regulatory regions (see STAR Methods, FDR < 0.05) (Figures 4C, S4B–C, Table S4). These included 497 cytokine-inducible NF-κB binding sites that were identified as NF-κB targets by p65 ChIP-seq in IL-1β-treated β cells (Table S5). Of note, the proportion of p65 peaks induced by IL-1β within loops was threefold higher than the background occurrence of NF-κB motifs found in all accessible cis-regulatory elements identified in our mouse islet ATAC-seq peakset (12% versus 4%). A prominent PDX1 chromatin loop was observed between a PDX1 binding site 2.1 kb upstream of *TNF receptor-associated factor 3 interacting protein 1* (*Traf3ip1*) and an NF-κB binding site within the 5' UTR of the *Per2* gene (Figure 4C). We also observed co-localization between PDX1 and NF-κB sites at genes involved in Ca^{2+} signaling (*Inpp4b*) and inflammation (*Irf2*)

(Figure S4C), as well as at other IL-1β-induced NF-κB sites such as the IL-1β receptor (*Il1r1*), tumor necrosis factor receptor-associated factor interacting protein (*Traf3ip2*), and the type 2 diabetes associated allele *Slc30a8* (Table S5). To test whether PDX1 inhibits NF-κB at these distal enhancers through recruitment of co-repressor complexes, we performed chromatin-immunoprecipitation with the transcriptional corepressor SIN3A, which establishes β-cell identity together with PDX1[60]. Of the 4,925 sites bound by SIN3A, 41% co-localized with PDX1-regulated genes, including *Traf3ip1* and TNF-related genes such as *Tnfsf4* and *Traf5* (Table S6, Figures 4C, S4C–D)[61]. Moreover, we found that loss of PDX1 disrupts SIN3A chromatin binding genome-wide (Figure S4E), including reduced SIN3A binding at IL-1β inducible NF-κB binding sites near the gene encoding *Nfkbie* (Figure S4F). Of note, this region also undergoes long-range chromatin contacts with PDX1 binding sites (Figure S4F), consistent with PDX1 repression of NF-κB across long distances via three-dimensional interactions and co-recruitment of SIN3A.

Inhibition of NF-κB signaling using an IL-1β-receptor antagonist enhances β-cell function in Pdx1-deficient β cells

Human PDX1^{low} and murine *Pdx1*$^{\Delta AIV/-}$ β cells both exhibit signatures of increased chromatin openness at pro-inflammatory networks and NF-κB targets such as interleukin-1β (IL-1β) (Figures 1–2). The IL-1 receptor (IL-1R) is one of the most highly expressed cytokine receptors within pancreatic islet β cells[62]. Exposure to IL-1β remodels the β-cell chromatin landscape[63], and antagonism of IL-1β represents a well-established anti-inflammatory strategy in humans[64,65]. Inflammation also appears to play a role in β-cell dysfunction in type 2 diabetes through mechanisms that remain uncertain[66]. We found that IL-1β stimulation of β cells from wild-type mice induced the expression of canonical NF-κB targets (including *Nfkbiz* and *Nfkbia*) and repressed the expression of PDX1 targets (including *Mafa*, *Glp1r*, and *Pdx1* itself) (Figures 4D, S4G)[67]. IL-1β also inhibited glucose-stimulated insulin release in wild-type Beta-TC-6 cells (Figure 4E). Conversely, treatment of islets isolated from *Pdx1*$^{\Delta AIV/-}$ mutant mice with an IL-1β receptor antagonist (IL-1RA) robustly enhanced insulin secretion (Figure 4G), consistent with therapeutic amelioration of PDX1 deficiency through blockade of IL-1β-induced NF-κB signaling. We used hyperglycemic clamping to directly investigate whether blocking IL-1β might overcome hypoinsulinemia in *Pdx1* hypomorphic animals *in vivo*[68]. We evaluated differences in insulin-mediated glucose-infusion rates (GIRs) following stabilization of GIR (>50 min post-initiation of infusion) and assessed genotype-drug interactions. Our analysis revealed genotype-dependent differences in IL-1β receptor antagonist-treated animals versus vehicle (PBS) controls, with a trend towards an increased GIR in the IL-1β receptor antagonist-treated vs PBS-treated mutants. Hyperglycemic clamp results therefore suggest that antagonism of IL-1β has genotype-specific effects on glucose clearance in *Pdx1* hypomorphic animals (Figure S4H). Finally, anti-inflammatory treatment using the IL-1β receptor antagonist enhanced insulin secretion in *Bmal1* KO cells (Figure S4I). Altogether, our epigenomic and genetic studies indicate that blocking inflammation upstream of NF-κB may provide a novel insulinotropic therapy in states of β-cell failure related to PDX1 and/or clock dysfunction.

DISCUSSION

We have identified a unique β-cell subtype of adult islet cells with inflammatory transcriptional activity characterized by genome-wide enrichment of NF-κB networks concurrent with reduced activity of the master lineage regulator PDX1. Identification of this new islet subtype at single-cell resolution was possible because of the high mapping density of chromatin accessibility and resolution of specific regulatory elements across human islet subpopulations. Using three-dimensional chromosome conformation capture, we further showed that PDX1 represses inflammatory signaling through long-range inhibition of NF-κB and recruitment of the canonical co-repressor SIN3A. Conversely, we showed that de-repression of NF-κB in single islet cells from genetic models of *Pdx1* deficiency leads to β-cell failure and diabetes. These results *indicate that PDX1 protects the* β *cell from stress and inflammation and provide evidence for the cross-regulation of* PDX1 and pro-inflammatory/NF-κB signaling as a key element in β-cell function.

Our studies also revealed that PDX1 induces circadian gene networks important in metabolic homeostasis in mature β cells. We observed that PDX1 localizes to CLOCK/BMAL1 regulatory elements through a mechanism that varied across the circadian time-scale in both mice and humans. The observation that PDX1 binding sites were enriched within CLOCK/BMAL1 enhancers is consistent with prior studies that clock factors are involved in islet maturation and response to injury[13,24,69] and the repression of latent NF-κB-mediated inflammatory networks[59,70,71]. Our analyses further suggest that PDX1 promotes time-of-day-dependent activity of insulin exocytic gene networks while simultaneously repressing inflammatory signatures[70]. Varied conditions, such as overnutrition or aging itself, have been shown to alter circadian programming in a tissue-specific manner[72, 73]. Similarly, our genomic studies in *Bmal1* KO β cells revealed mixed effects of the clock factor BMAL1 on NF-κB-mediated gene expression. Specifically, ablation of *Bmal1* altered p65 binding to DNA at cell survival and anti-apoptotic genes (Figure S3G), whereas ablation of BMAL1 did not alter the binding of p65 to cytokine-induced inflammatory genes (Figure S3G). Previous work has demonstrated that p65/NF-κB is required for β-cell function, so it is possible that loss of p65 binding in BMAL1-ablated β cells contributes to the hypoinsulinemia in these animals, perhaps due to anti-apoptotic actions of the NF-κB pathway[74,75]. Future studies will be required to understand β-cell-specific responses to inflammatory stimuli throughout the circadian cycle and how core circadian activators or downstream clock-controlled genes interact with PDX1.

Human and animal studies have shown that disrupted clock function resulting from obesogenic diet and/or mistiming of feeding contributes to metabolic disease[76]. The data presented here suggests that IL-1β induction, which has been shown to increase with diet-induced obesity[59,77,78], may in turn trigger β-cell failure. Genetic PDX1 deficiency led to de-repression of latent NF-κB enhancers and provided rationale to inhibit IL-1β as an insulinotropic therapy. While prior studies have shown that IL-1β control of glucose homeostasis involves the central nervous system[66,79,80], our results in β-cell lines indicate that blocking IL-1β in enhances insulin secretion directly within the islet. Since human islets used in our studies were harvested from glucose-responsive donors, future studies will be

necessary to determine whether the antagonist relationship between PDX1 and NF-κB is disrupted in type 1 or type 2 diabetes.

Limitations of Study

Our experiments in human islets identified a link between PDX1, NF-κB, and the clock, though additional snATAC-seq and snRNA-seq studies will be required to determine whether the daily rhythms in chromatin accessibility in whole islets arise due to variation within individual β cells versus non β cells and whether the chromatin changes correspond with gene expression changes at the level of single cells. Further, while we found evidence of β-cell heterogeneity in both male and female subjects in our human islet studies, further studies will be required to specifically examine the effects of both sex and age in the *Pdx1* mutant animals. Our glucose tolerance experiments likewise provided evidence of a significant interaction between circadian time, *Pdx1* genotype, and glucose excursion, with a maximal difference in insulin release during the dark period. Given the controls used for these experiments were *Pdx1* heterozygotes, additional studies will be needed to compare how the *Pdx1* heterozygotes and Area IV mutants compare to wild-type controls[81,7]. Finally, future studies in preclinical context should seek to address whether loss of the clock or of lineage-determining factors predisposes animals to an inappropriate inflammatory response through a potential immunoendocrine mechanism.

STAR METHODS

RESOURCE AVAILABILITY

Lead Contact: Further information and requests for resources and reagents should be directed to and will be fulfilled by the lead contact, Joseph Bass (j-bass@northwestern.edu).

Materials Availability: This study did not generate new unique reagents.

Data and Code Availability:

- Data in this study is publicly available in the GEO repository (GSE 214678). All unprocessed data can be found in Data S1 – Source Data.
- This paper does not report original code.
- Any additional information required to reanalyze the data reported in this paper can be found in the Key Resources Table and is available from the lead contact upon request.

EXPERIMENTAL MODEL AND SUBJECT DETAILS

Mice—Male $Pdx1^{+/-}$ control and $Pdx1^{\Delta AIV/-}$ mutant mice (provided by Dr. Roland Stein, Vanderbilt University), as well as $PdxCre;Bmal1^{fx/fx}$ mice, were maintained on a C57BL/6J background at the Northwestern University Center for Comparative Medicine[7,12]. $Pdx1^{+/-}$ and $Pdx1^{\Delta AIV/-}$ mice were crossed with $Per2^{Luc}$ mice[82] to generate $Pdx1^{+/-};Per2^{Luc}$ and $Pdx1^{\Delta AIV/-};Per2^{Luc}$ mice. All animals were maintained on a 12:12 light:dark cycle and allowed free access to water and regular chow unless otherwise indicated. All animal care

and use procedures were conducted in accordance with regulations of the Institutional Animal Care and Use Committee at Northwestern University.

Beta-TC-6 cell culture—Beta-TC-6 cells (ATCC) and *Bmal1* KO cells[83] were cultured in Dulbecco's Modified Eagle's Medium (DMEM) supplemented with 15% fetal bovine serum, 1% penicillin-streptomycin, and 1% L-glutamine at 37°C with 5% CO_2. Culture medium was exchanged every two to three days. All cells used in these experiments were <15 passages and were routinely checked for mycoplasma contamination.

METHOD DETAILS

Single-nuclei ATAC-seq sample prep—Human islets were obtained from the Integrated Islet Distribution Program (IIDP) and are listed under RRIDS: SAMN17928660, SAMN25519947, and SAMN25980818 (Table S7). Approximately 200 human islet equivalents (IEQs) were cultured in RPMI supplemented with 10% human AB serum, 1% penicillin/streptomycin, and 1% glutamine at 5% CO_2 for two days prior to 10X processing. Mouse islets were obtained and pooled from 2–3 animals to acquire ~200 IEQs and maintained in in RPMI supplemented with 10% heat-inactivated fetal bovine serum (FBS), 1% penicillin/streptomycin, and 1% glutamine at 5% CO_2. Both human and mouse islets were dissociated into single cells using gentle trituration at 3 min and 6 min for a total of 6 minutes of trypsin-EDTA treatment at 37°C with 600 rpm rotation. Trypsin digestion was then quenched with media and passed through a 40 μm Flowmi cell strainer to obtain a single cell suspension. Cells were then pelleted at 500g for 5 min followed by two washes with 1X PBS + 0.04 % BSA. Cells were resuspended in 100 μL 1X lysis buffer (10 mM pH 7.4 Tris-HCl, 10 mM NaCl, 3 mM $MgCl_2$, 0.1% Tween-20, 0.1% Tergitol, 0.01% digitonin, and 1% BSA) and incubated on ice for 3 min, immediately followed by 5x passages through a 1 mL insulin needle (31 gauge) to fully lyse membranes. Nuclei were then dispensed into 1 mL lysis wash buffer (10 mM pH 7.4 Tris-HCl, 10 mM NaCl, 3 mM $MgCl_2$, 0.1% Tween-20, and 1% BSA) and pipetted to mix. Nuclei were pelleted at 500g for 5 min and resuspended in 1X nuclei buffer (10X Genomics) for viability staining and counting. Nuclei were then subjected to transposition, gel bead-in-emulation (GEM) generation, and cell-barcoding according to manufacturer's recommendations.

Single-nuclei-sequencing library sequencing, alignment, and quantitation—Libraries were amplified and barcoded using 9–11 cycles of PCR. Average base pair size and library quality were determined using Bioanalyzer, and library concentrations quantity were determined using Qubit. Libraries were then subjected to paired-end sequencing using 34×34 paired-end reads, 8 cycles for i7, and 16 cycles for i5 index for barcode and UMI demultiplexing. snATAC samples were demultiplexed and aligned to reference genomes (Hg38 or mm10) using Cell Ranger ATAC (v2.0.0) for ATAC or Cell Ranger (v6.1.2) for 10X RNA-seq (GSE114297) using the "mkfastq" followed by "count" then "aggr" commands to generate nonnormalized individual and aggregate feature count by cell-barcode matrices for input into R.

Single-cell clustering and variable feature analysis—The analytical pipeline has been made publicly available and was performed using R version 4.1.2. In brief, snATAC

peak matrices and cell metadata were read into Seurat (v4.1.0). Following low-quality cell removal (cells with either <15% reads in peaks, blacklist ratio > 0.05, nucleosome signal > 4, or transcription start site enrichment < 2), UMAP clustering was performed. For human preparations, Harmony[84] integration was first performed on a PCA reduction. For both mouse and human snATAC samples, UMAP reduction and clustering was then performed to identify distinct cell clusters. Variable features for cell type identification and analysis were used following peak annotation (ChIPseeker, v1.31.3) and quantification of gene activity was scored as the sum of accessible reads at fragments overlapping gene coordinates and the 2 kb region upstream (hg38 and mm10). To identify variable TF signatures, we assessed TF activity using chromVAR (v1.16.0) to measure TF-associated chromatin accessibility using position weight matrices from both mouse and human TF motifs annotated in the JASPAR 2020 database[26]. UMAP coordinates were used in performing coaccessbility analysis via cicero (v1.3.5). Significant features enriched between cell clusters or genotypes were determined using a likelihood ratio test from comparing a logistic regression for gene activity, peak accessibility, or TF accessibility as appropriate[85]. Pathway enrichment analysis was performed for differential gene activities between mouse genotypes was performed using Metascape with terms “KEGG” and “Gene Ontology Pathways” included for analysis.

RNAscope multiplex analysis—Paraffin-embedded human pancreas slides (human RRIDs: SAMN12227196, SAMN17928660, SAMN25519947) were obtained from IIDP. Multiplex RNAscope hybridization was done by the Northwestern University Research Histology and Phenotyping Laboratory. Briefly, tissue sections were dewaxed, treated with 3% H_2O_2 for 10 min and incubated at 95°C for 15 min in Target Retrieval Reagent (ACD Bio). Cooled slides were rinsed twice in 100% ethanol, dried for 5 min at 60°C, and marked with ImmEdge Hydrophobic Barrier pen. Slides were treated with RNAscope Protease Plus (ACD) for 30 min at 40°C, hybridized with human RNAscope probes for PDX1 and INS (ACD, Cat#43081, Cat#313571-C4, respectively) or Human RNAscope® 4-plex Positive Control Probes for RNAscope Multiplex Fluorescent Assay (*POLR2A*, *PPIB*, *UBC* and *HPRT1*) (ACD Cat#321801) and then with OPAL fluorophores OPAL 520, OPAL 620, OPAL 690 and OPAL Polaris 780 (Akoya Biosciences, Cat#FP1487001KT, Cat#FP1495001KT, Cat#FP1497001KT, Cat#FP1501001KT) for 2 hrs at 40°C, and processed for probe detection using RNA-scope Multiplex Fluorescent Detection Kit (ACD, Cat#323110). To control for background noise, slides were hybridized with RNAscope® 4-plex Multiplex Negative Control Probe were used every run (ACD Cat#321831). Following hybridization, all slides were mounted in Vectashield VIBRANCE Plus DAPI (Vector Labs) and imaged using Nikon Ti2 Widefield fluorescence microscope and NIS Elements Software (Nikon). To assess the distribution of β cells according to RNA abundance, images of 13–35 islets/donor were analyzed by quantifying fluorescence for each probe in individual cells using Fiji image processing package (ImageJ). Raw values for *PDX1*, *HPRT1*, *UBC*, *PPIB*, and *POLR2A*) were normalized to DAPI staining. Best fit for single- and multiple-component distributions was determined using the *fitdistrplus* and *mixtools* packages in R, respectively. Multiple components were considered for normalized expression value distributions which exhibit a significant deviation (P-Value < 0.05 by Kolmogorov–Smirnov test) from a single component Gaussian distribution.

Bulk ATAC-seq preparation and analysis—Mouse or human islets (10 IEQs per sample per timepoint, human RRIDs: SAMN13134368, SAMN13254972, SAMN13515839, SAMN13739565) were synchronized using a 10 μM forskolin pulse for 1 hour, followed by culturing in normal media for 24–48 hours as indicated. Single cell suspensions were obtained as described above. Following a brief ice-cold PBS wash, cells were resuspended and pipetted three times in 50 μL ice-cold resuspension buffer (10 mM Tris-HCl pH 7.4, 10 mM NaCl, 3 mM MgCl2) containing 0.1% IGEPAL, 0.1% Tween-20, and 0.01% digitonin. Cells were then pelleted and washed twice in resuspension buffer without detergent. Cells were then resuspended in 50 μL of ATAC-seq reaction buffer containing 1.25 μL transposase enzyme (TE, Illumina, FC-121–1030) in a 50 μL 1X transposition mix (25 μL 1X TD, 16.5 μL PBS, 0.5 μL 1% digitonin, 0.5 μL 10% Tween-20, 6.25 μL water) and incubated at 37°C for 30 minutes in a thermomixer with 1000 RPM mixing. The transposition reaction was immediately quenched and DNA purified using the Qiagen MinElute Reaction Cleanup Kit. Samples were eluted followed by amplification and barcoded using Nextera indexes for 8–10 cycles Q5 High-Fidelity 2X Master Mix. PCR-amplified libraries were then cleaned up using two-sided size selection (0.5X followed by 1.3X Ampure XP, per manufacturer's instruction). Library quality control and quantitation was performed using an Agilent 2100 Bioanalyzer. Libraries were sequenced using paired-end sequencing (42×42 bp) on a NextSeq 500. Following sequencing, library quality control and alignment to mm10 or hg38 was performed using the ENCODE pipeline. Peaks were called for individual merged samples using 150 bp peak width to identify open chromatin regions, followed by peak annotation and read quantitation using HOMER. Following removal of peaks with < 10 average counts per sample, we then performed differential peak analysis at filtered consensus peaks using the DESeq2 algorithm in R to identify significantly (FDR < 0.05) altered peak regions with respect to circadian time and/or genotype in a two-factor general linearized model using log-odd ratio testing. We compared significantly altered peaks against the filtered input peak list to identify enriched TF motifs using the findMotifsGenome.pl tool in HOMER. DESeq2 normalized counts were calculated and used for box- and barplots using the ggplot package within R. Rhythmic ATAC-seq analysis was performed using the approach previously utilized for analysis of human islet RNA-sequencing data[7]. In brief, normalized DESeq2 counts were transformed into Z-scores for each individual islet donor across the 24-hour timeseries. Z scores were then imported into eJTK_CYCLE using the provided 24-hour cosine wave parameter at a resolution of 2 hours to identify significantly rhythmic peaks (Bonferroni P-Value < 0.05).

ChIP-sequencing—Approximately 1×10^7 cells per replicate were fixed on tissue culture treated-plates in 2 mM disuccinimidyl glutarate in PBS + 1% DMSO for 30 min, followed by formaldehyde (1% in PBS) cross-linking for 10 min, followed by quenching to a final concentration of 125 mM glycine. Nuclei were isolated in lysis buffer (150 mM NaCl, 5 mM EDTA at pH 8, 50 mM Tris-HCl at pH 8, 0.35% NP-40) using five passages through a needle and syringe in buffer in the presence of Roche Mini EDTA-free protease inhibitor cocktail. Nuclei were pelleted at 2000 × g for 5 min to obtain a rough nuclear isolate. Chromatin was sheared using a Covaris M220 with 75 W power; 10% duty factor, 200 cycle per burst, 4-minute total time at 4°C, in shearing buffer (1% SDS, 2.5 mM EDTA at pH 8, 50 mM Tris-HCl at pH 8). Dilution buffer (0.01% SDS, 1.1% Triton X-100, 167

mM NaCl, 1.2 mM EDTA at pH 8, 1.67 mM Tris-HCl at pH 8) was added 9:1 for dilution and antibodies added (10 μL anti-p65, CST#8242; 10 μL anti-PDX1, CST#5679; Millipore ABE2599, anti-SIN3A, CST#8056S), followed by rotation overnight at 4°C. Secondary antirabbit (for anti-p65 and anti-PDX1) magnetic beads were added (40 μL) and incubated for an additional 6 hours at 4°C with rotation. Magnetic beads were washed 6 times in lysis buffer followed by one additional wash in 1X TE. Two bead elutions were carried out at 25°C in 100 μL of 100 mM $NaHCO_3$ and 1% SDS for 30 min with 1000 rpm rotation. Eluted DNA was then reverse crosslinked with the addition of 8 μL NaCl (5 M) and rotation at 65°C overnight. ChIP DNA was then treated with 1 μL of 10 μg/mL RNAase A and 1 μL of 10 μg/mL of proteinase K for a total of 1 hour at 37°C and purified using the Qiagen MinElute kit. Libraries were then prepared for sequencing using the NEBNext Ultra II library preparation kit, size-selected using Sage Pippin PrepHT for fragments between 200 and 600 bp. Libraries were indexed and amplified for 11 cycles of PCR followed by DNA purification using 0.9 × Ampure XP bead size selection, analyzed for quality and base pair size using an Agilent 2100 Bioanalyzer, and sequenced on an Illumina Nextseq 500 using 75-bp single-end reads for more than 20 million unique reads aligned per sample. Raw sequencing reads were aligned to the mm10 genome using Bowtie2 (v2.2.4) with default parameters. Peaks were called for each sample relative to sheared DNA input using the “findPeaks” function in HOMER with the optional “-style factor” parameter. A differential peak threshold of >2-fold change above input (for peak identification) or relative to control (for siRNA experiments) was considered significant. The “mergePeaks” function in HOMER was used to identify unique peaks identified between SIN3A ChIP-seq peaks. Enriched TF motifs (taken from JASPAR2020) were detected using the findMotifsGenome.pl tool in HOMER using an FDR cut-off of 0.05. Differential peak analysis was performed at filtered consensus peaks with raw tag counts >10 using the DESeq2 algorithm in R to identify significantly altered binding (FDR < 0.05). HOMER normalized tag counts were imported into R to generate scatter and boxplots.

HiChIP-sequencing—Cells were prepared according to the absolute quantification of architecture HiChIP (AQuA-HiChIP), with a few modifications as noted below[86]. 1 × 107 cells per replicate were fixed on 15-cm tissue-culture treated plates in formaldehyde (1% in PBS), followed by quenching to a final concentration of 125 mM glycine. Cells were lysed in lysis buffer (150 mM NaCl, 5 mM EDTA at pH 8, 50 mM Tris-HCl at pH 8, 0.35% NP-40) using five passages through a needle and syringe in buffer in the presence of Roche Mini EDTA-free protease inhibitor cocktail. Rough nuclei were pelleted at 2000 × g for 5 min and then resuspended in 0.5% SDS in TE pH 7.4, incubated at 62°C, and quenched with 10% Triton X-100. MboI digestion was performed followed by overhang blunting and biotinylation using biotin-dATP. Ligation using T4 DNA ligase for 4 hours at room temperature followed by overnight at 4°C. Chromatin was pelleted and then lysed and sheared using a Covaris M220 with 75 W power; 10% duty factor, 200 cycle per burst, 4-minute total time at 4°C) in shearing buffer (1% SDS, 2.5 mM EDTA at pH 8, 50 mM Tris-HCl at pH 8). Dilution buffer (0.01% SDS, 1.1% Triton X-100, 167 mM NaCl, 1.2 mM EDTA at pH 8, 1.67 mM Tris-HCl at pH 8) was added 9:1 for dilution and anti-PDX1 added overnight at 4°C with rotation (10 μL anti-PDX1, CST#5679), followed by 6-hour secondary incubation using anti-rabbit IgG Dynabeads. Following bead washing, elution,

decrosslinking and purification using MiniElute columns (see above), streptavidin M280 Dynabeads were prewashed twice in Tween Wash Buffer (5 mM Tris-HCl pH 8.0, 0.5 mM EDTA, 1 M NaCl, 0.05% Tween-20), resuspended in 2 × Biotin Binding Buffer, and added to reverse crosslinked DNA to bind biotinylated fragments. Following bead binding, beads were washed 3 × times in Tween Wash Buffer followed by 3 × washes with TE pH 7.4. Library preparation was performed as above for ChIP-seq, without size selection. Libraries were sequenced using 42×42 bp paired end sequencing using an Illumina NextSeq 500. Data analysis was performed using the AquA-HiChIP pipeline using HiC-Pro (v3.1.0) followed by Juicer (v1.6)[87]. Valid pair files were processed using HiCExplorer (v2.2) followed by analysis in R using the package rtracklayer to generate genome browser tracks alongside ChIP-seq samples[88]. Significant interactions were determined using mouse bulk ATAC-Seq peaks or IL-1β inducible p65 peaks using the "Peak2Peak" option via FitHiChIP (v8.0) and using an FDR P-Value cutoff < 0.05[89]. Significant interactions were visualized using the WashU Epigenome Browser.

RNA isolation and RNA-sequencing—Cells (or islets) were rapidly lysed in 350 μL TRI reagent, vortexed for 10s at high speed, frozen, and processed for RNA isolation using using Direct-zol miniprep columns (Zymo) with DNA digestion. mRNA libraries were prepared using either NEBNext Ultra II Directional RNA Library Prep Kits (New England Biolabs) with poly(A) enrichment for cells, or the NEBNext Single Cell/Low Input RNA Library Prep Kit for islets. Libraries were sequenced to a depth > 15M reads per library using 75–100 bp single-end reads. Reads were mapped to the mm10 genome using annotations from gencode vM10 assembly with STAR version 2.5.0 followed by quantification using RSEM version 1.3.3 using default parameters. Differential expression was carried out using DESeq2 with default parameters, and pathway analysis was performed using Metascape and *pathfindR* (v2.3.0).

***Pdx1* knockdown and IL-1β treatment in Beta-TC6 cells—**Knockdown of Pdx1 was performed in Beta-TC6 cells using reverse transfection in OptiMEM by adding 12 pmol anti-Pdx1 siRNA (ThermoFisher) or control siRNA (ThermoFisher Select Negative Control No. 1 siRNA) per well and 7.5 μL of Lipofectamine 3000 per well of a 6-well dish for RNA. For ChIP, transfection was performed in 10 cm tissue-cultured plates using 70 pmol siRNA and 43.5 μL lipofectamine. Cells were then plated at 5×10^5 cells/well for RNA and 5×10^6 for ChIP. For Western blots, transfection was performed in 6 cm plates using 33 pmol siRNA again 15 μL of Lipofectamine 3000, and cells were plated at 4×10^5 cells/dish. 48 hours post-transfection, cells were treated with recombinant IL-1β (BioLegend) for 2 hours at a final concentration of 0.1 ng/mL in normal media (DMEM supplemented with 5% FBS, 1% glutamine, and 1% penicillin/streptomycin) and harvested for RNA-seq, ChIP-seq, qPCR, or Western blots.

Nuclear and cytoplasmic fractionation and Western blotting—Cytoplasmic and nuclear proteins were harvested using NE-PER Nuclear and Cytoplasmic Reagent Kit (Thermo Fisher Scientific) with the following modifications: nuclear pellets were vortexed for 15 sec in the NER1 buffer with HALT Protease and Phosphatase Inhibitors (Thermo Fisher Scientific) and then sonicated at 4°C for 3–6 cycles of 30 sec pulses. Samples

were spun at 16,000g for 10 min and supernatants were stored at −80°C. Protein levels were quantified using BioRad DC Protein Assay and protein expression was analyzed with Western blotting using 20 μg of each fraction. The Immobolin-P Membrane (Sigma) was hybridized to the following antibodies: PDX1, NF-κB p65, Histone H3, GAPDH, and HRP-linked anti-rabbit IgG (Cell Signaling, Cat#5679, Cat#8242, Cat#9715, Cat#5174, Cat#7074, respectively). Signal was detected using Super Signal West PICO PLUS Chem-Illuminescent Substrate (Thermo Fisher Signaling) and X-ray film.

Insulin secretion assays in pancreatic islets, pseudoislets, and cell lines— Mouse pancreatic islets were isolated via bile duct collagenase digestion (*Collagenase P*, Sigma) and Biocoll (Millipore) gradient separation and left to recover overnight at 37°C in RPMI 1640 with 10% FBS, 1% L-glutamine, and 1% penicillin/streptomycin. For insulin release assays, duplicates of 5 islets of equal size per mouse were statically incubated in Krebs-Ringer Buffer (KRB) at 2 mM glucose for 1 hr, then stimulated for 1 hr at 37°C with 2 mM or 20 mM glucose in the presence or absence of 0.5 μg/mL murine Interleukin-1 receptor antagonist (Sigma). Supernatant was collected and assayed for insulin content by ELISA (Crystal Chem Inc). Islets were then sonicated in acid-ethanol solution and solubilized overnight at 4°C before assaying total insulin content by ELISA. For insulin release assays from pseudoislets, *Pdx1* knockdown in Beta-TC-6 cells was achieved as described above. Then, 3×10^6 cells were plated for 3 days in 60 mm suspension dishes and allowed to form pseudoislets. Glucose-responsive insulin secretion was performed as described above, using 10 pseudoislets per sample and a basal glucose level of 0 mM glucose instead of 2 mM. When indicated, 0.1 ng/mL recombinant mouse IL-1β was used.

Oral glucose tolerance tests and hyperglycemic clamps—Mice were fasted for 14 hrs, and glucose tolerance tests were performed at ZT2 and ZT14 following glucose administration of 2 g/kg body weight through oral gavage. Blood glucose was measured at indicated times by hand-held meter, and plasma insulin and C-peptide levels were measured by ELISA (Crystal Chem Inc). Hyperglycemic clamps were performed in 5 hr fasted chronically catheterized (carotid artery and jugular vein) conscious mice at the Vanderbilt Mouse Metabolic Phenotyping Center[90, 91]. Blood was obtained from the carotid artery and glucose was infused into the jugular vein to raise and maintain arterial glucose levels around 280 mg/dl. Washed red blood cells were infused to replace blood removed for serial sampling.

LumiCycle analysis—Approximately 100–150 pancreatic islets from $Pdx1^{+/-}$;$Per2^{Luc}$ and $Pdx1^{\Delta AIV/-}$; $Per2^{Luc}$ mice were isolated as described above. Islets were then cultured on tissue culture membranes in modified DMEM[7]. Sealed cultures were placed at 37°C in a LumiCycle luminometer (Actimetrics), and sample bioluminescence was recorded continuously. After several days in culture, islets were synchronized by the addition of 10 μM forskolin for 1 hr, followed by incubation in fresh media. Period length was calculated via a modified best-fit sine wave analysis using LumiCycle analysis software (Actimetrics).

QUANTIFICATION AND STATISTICAL ANALYSIS

Statistical analyses—Data was analyzed using R (v4.1.2) and Prism (v9.0). Differential analysis of single-cell sequencing data was performed using the Seurat (v4.1.0) package in R (v4.0.1) using the likelihood-ratio test ("LRT") method with minimum "percent expressed" set to 0.10 and "minimum difference in percent expressed" set to 0.05. Two-way ANOVAs were used to analyze insulin secretion and GTTs, followed by Holm-Šídák multiple comparison testing. The "lme4" package (v1.1) was used to assess the effect of genotype and drug in the hyperglycemic clamping data by using a mixed linear model and setting time as fixed random effect (https://www.jstatsoft.org/article/view/v067i01).

Supplementary Material

Refer to Web version on PubMed Central for supplementary material.

ACKNOWLEDGEMENTS

We thank all the members of the Bass, Barish, and Beutler laboratories for helpful discussions. Histology services were provided by the Northwestern University Mouse Histology and Phenotyping Laboratory and the Northwestern University Center for Advanced Microscopy which are supported by NCI P30-CA060553 awarded to the Robert H Lurie Comprehensive Cancer Center. This work was supported by the Northwestern University NUSeq Core Facility. Research support was from the NIH National Institute of Diabetes and Digestive and Kidney Diseases (NIDDK) grants R01DK127800, R01DK113011, R01DK090625, and R01DK050203 and the National Institute on Aging (NIA) grant R01AG065988 and P01AG011412, as well as the University of Chicago Diabetes Research and Training Center grant P30DK020595 (to J.B.); NIDDK grant F30DK116481 (to B.J.W.); NIDDK grant F31DK130589 (to N.J.W.); NIDDK grants U24DK059637 and P30DK020593 (to L.L. and O.P.M); and NIDDK grant R01DK050203 (to R.W.S.).

REFERENCES:

1. Heinz S, Benner C, Spann N, Bertolino E, Lin YC, Laslo P, Cheng JX, Murre C, Singh H, and Glass CK (2010). Simple combinations of lineage-determining transcription factors prime cis-regulatory elements required for macrophage and B cell identities. Mol Cell 38, 576–589. [PubMed: 20513432]
2. Wortham M, and Sander M (2021). Transcriptional mechanisms of pancreatic beta-cell maturation and functional adaptation. Trends Endocrinol Metab 32, 474–487. [PubMed: 34030925]
3. Chiou J, Zeng C, Cheng Z, Han JY, Schlichting M, Miller M, Mendez R, Huang S, Wang J, Sui Y, et al. (2021). Single-cell chromatin accessibility identifies pancreatic islet cell type- and state-specific regulatory programs of diabetes risk. Nat Genet 53, 455–466. [PubMed: 33795864]
4. Chiou J, Geusz RJ, Okino ML, Han JY, Miller M, Melton R, Beebe E, Benaglio P, Huang S, Korgaonkar K, et al. (2021). Interpreting type 1 diabetes risk with genetics and single-cell epigenomics. Nature 594, 398–402. [PubMed: 34012112]
5. Fasolino M, Schwartz GW, Patil AR, Mongia A, Golson ML, Wang YJ, Morgan A, Liu C, Schug J, Liu J, et al. (2022). Single-cell multi-omics analysis of human pancreatic islets reveals novel cellular states in type 1 diabetes. Nat Metab 4, 284–299. [PubMed: 35228745]
6. Gao T, McKenna B, Li C, Reichert M, Nguyen J, Singh T, Yang C, Pannikar A, Doliba N, Zhang T, et al. (2014). Pdx1 maintains beta cell identity and function by repressing an alpha cell program. Cell Metab 19, 259–271. [PubMed: 24506867]
7. Perelis M, Marcheva B, Ramsey KM, Schipma MJ, Hutchison AL, Taguchi A, Peek CB, Hong H, Huang W, Omura C, et al. (2015). Pancreatic beta cell enhancers regulate rhythmic transcription of genes controlling insulin secretion. Science 350, aac4250.
8. Boj SF, Parrizas M, Maestro MA, and Ferrer J (2001). A transcription factor regulatory circuit in differentiated pancreatic cells. Proc Natl Acad Sci U S A 98, 14481–14486. [PubMed: 11717395]

9. Hunter CS, and Stein RW (2017). Evidence for Loss in Identity, De-Differentiation, and Trans-Differentiation of Islet beta-Cells in Type 2 Diabetes. Front Genet 8, 35. [PubMed: 28424732]
10. Yang YP, Thorel F, Boyer DF, Herrera PL, and Wright CV (2011). Context-specific alpha- to-beta-cell reprogramming by forced Pdx1 expression. Genes Dev 25, 1680–1685. [PubMed: 21852533]
11. Pullen TJ, Khan AM, Barton G, Butcher SA, Sun G, and Rutter GA (2010). Identification of genes selectively disallowed in the pancreatic islet. Islets 2, 89–95. [PubMed: 21099300]
12. Spaeth JM, Gupte M, Perelis M, Yang YP, Cyphert H, Guo S, Liu JH, Guo M, Bass J, Magnuson MA, et al. (2017). Defining a Novel Role for the Pdx1 Transcription Factor in Islet beta-Cell Maturation and Proliferation During Weaning. Diabetes 66, 2830–2839. [PubMed: 28705881]
13. Petrenko V, Stolovich-Rain M, Vandereycken B, Giovannoni L, Storch KF, Dor Y, Chera S, and Dibner C (2020). The core clock transcription factor BMAL1 drives circadian beta-cell proliferation during compensatory regeneration of the endocrine pancreas. Genes Dev 34, 1650–1665. [PubMed: 33184223]
14. Rai V, Quang DX, Erdos MR, Cusanovich DA, Daza RM, Narisu N, Zou LS, Didion JP, Guan Y, Shendure J, et al. (2020). Single-cell ATAC-Seq in human pancreatic islets and deep learning upscaling of rare cells reveals cell-specific type 2 diabetes regulatory signatures. Mol Metab 32, 109–121. [PubMed: 32029221]
15. Miguel-Escalada I, Bonas-Guarch S, Cebola I, Ponsa-Cobas J, Mendieta-Esteban J, Atla G, Javierre BM, Rolando DMY, Farabella I, Morgan CC, et al. (2019). Human pancreatic islet three-dimensional chromatin architecture provides insights into the genetics of type 2 diabetes. Nat Genet 51, 1137–1148. [PubMed: 31253982]
16. Yang X, Raum JC, Kim J, Yu R, Yang J, Rice G, Li C, Won KJ, Stanescu DE, and Stoffers DA (2022). A PDX1 cistrome and single-cell transcriptome resource of the developing pancreas. Development 149.
17. Gaulton KJ, Ferreira T, Lee Y, Raimondo A, Magi R, Reschen ME, Mahajan A, Locke A, Rayner NW, Robertson N, et al. (2015). Genetic fine mapping and genomic annotation defines causal mechanisms at type 2 diabetes susceptibility loci. Nat Genet 47, 1415–1425. [PubMed: 26551672]
18. van de Bunt M, Manning Fox JE, Dai X, Barrett A, Grey C, Li L, Bennett AJ, Johnson PR, Rajotte RV, Gaulton KJ, et al. (2015). Transcript Expression Data from Human Islets Links Regulatory Signals from Genome-Wide Association Studies for Type 2 Diabetes and Glycemic Traits to Their Downstream Effectors. PLoS Genet 11, e1005694. [PubMed: 26624892]
19. Avrahami D, Wang YJ, Schug J, Feleke E, Gao L, Liu C, Consortium H, Naji A, Glaser B, and Kaestner KH (2020). Single-cell transcriptomics of human islet ontogeny defines the molecular basis of beta-cell dedifferentiation in T2D. Mol Metab 42, 101057. [PubMed: 32739450]
20. Zhang K, Hocker JD, Miller M, Hou X, Chiou J, Poirion OB, Qiu Y, Li YE, Gaulton KJ, Wang A, et al. (2021). A single-cell atlas of chromatin accessibility in the human genome. Cell 184, 5985–6001 e5919. [PubMed: 34774128]
21. Geusz RJ, Wang A, Chiou J, Lancman JJ, Wetton N, Kefalopoulou S, Wang J, Qiu Y, Yan J, Aylward A, et al. (2021). Pancreatic progenitor epigenome maps prioritize type 2 diabetes risk genes with roles in development. Elife 10.
22. Preissl S, Gaulton KJ, and Ren B (2022). Characterizing cis-regulatory elements using single-cell epigenomics. Nat Rev Genet.
23. Wang YJ, and Kaestner KH (2019). Single-Cell RNA-Seq of the Pancreatic Islets--a Promise Not yet Fulfilled? Cell Metab 29, 539–544. [PubMed: 30581120]
24. Alvarez-Dominguez JR, Donaghey J, Rasouli N, Kenty JHR, Helman A, Charlton J, Straubhaar JR, Meissner A, and Melton DA (2020). Circadian Entrainment Triggers Maturation of Human In Vitro Islets. Cell Stem Cell 26, 108–122 e110. [PubMed: 31839570]
25. Xin Y, Dominguez Gutierrez G, Okamoto H, Kim J, Lee AH, Adler C, Ni M, Yancopoulos GD, Murphy AJ, and Gromada J (2018). Pseudotime Ordering of Single Human beta-Cells Reveals States of Insulin Production and Unfolded Protein Response. Diabetes 67, 1783–1794. [PubMed: 29950394]
26. Muto Y, Wilson PC, Ledru N, Wu H, Dimke H, Waikar SS, and Humphreys BD (2021). Single cell transcriptional and chromatin accessibility profiling redefine cellular heterogeneity in the adult human kidney. Nat Commun 12, 2190. [PubMed: 33850129]

27. Schep AN, Wu B, Buenrostro JD, and Greenleaf WJ (2017). chromVAR: inferring transcription-factor-associated accessibility from single-cell epigenomic data. Nat Methods 14, 975–978. [PubMed: 28825706]
28. Ahlgren U, Jonsson J, Jonsson L, Simu K, and Edlund H (1998). beta-cell-specific inactivation of the mouse Ipf1/Pdx1 gene results in loss of the beta-cell phenotype and maturity onset diabetes. Genes Dev 12, 1763–1768. [PubMed: 9637677]
29. Fang B, Everett LJ, Jager J, Briggs E, Armour SM, Feng D, Roy A, Gerhart-Hines Z, Sun Z, and Lazar MA (2014). Circadian enhancers coordinate multiple phases of rhythmic gene transcription in vivo. Cell 159, 1140–1152. [PubMed: 25416951]
30. Takahashi JS (2017). Transcriptional architecture of the mammalian circadian clock. Nat Rev Genet 18, 164–179. [PubMed: 27990019]
31. Medzhitov R, and Horng T (2009). Transcriptional control of the inflammatory response. Nat Rev Immunol 9, 692–703. [PubMed: 19859064]
32. Fan G, Sun L, Shan P, Zhang X, Huan J, Zhang X, Li D, Wang T, Wei T, Zhang X, et al. (2015). Loss of KLF14 triggers centrosome amplification and tumorigenesis. Nat Commun 6, 8450. [PubMed: 26439168]
33. Satpathy AT, Granja JM, Yost KE, Qi Y, Meschi F, McDermott GP, Olsen BN, Mumbach MR, Pierce SE, Corces MR, et al. (2019). Massively parallel single-cell chromatin landscapes of human immune cell development and intratumoral T cell exhaustion. Nat Biotechnol 37, 925–936. [PubMed: 31375813]
34. Zhu Y, Liu Q, Zhou Z, and Ikeda Y (2017). PDX1, Neurogenin-3, and MAFA: critical transcription regulators for beta cell development and regeneration. Stem Cell Res Ther 8, 240. [PubMed: 29096722]
35. Fukuda A, Kawaguchi Y, Furuyama K, Kodama S, Horiguchi M, Kuhara T, Kawaguchi M, Terao M, Doi R, Wright CV, et al. (2008). Reduction of Ptf1a gene dosage causes pancreatic hypoplasia and diabetes in mice. Diabetes 57, 2421–2431. [PubMed: 18591390]
36. Schaffer AE, Freude KK, Nelson SB, and Sander M (2010). Nkx6 transcription factors and Ptf1a function as antagonistic lineage determinants in multipotent pancreatic progenitors. Dev Cell 18, 1022–1029. [PubMed: 20627083]
37. Kharchenko PV (2021). The triumphs and limitations of computational methods for scRNA-seq. Nat Methods 18, 723–732. [PubMed: 34155396]
38. Wang H, Yang Z, Li X, Huang D, Yu S, He J, Li Y, and Yan J (2020). Single-cell in vivo imaging of cellular circadian oscillators in zebrafish. PLoS Biol 18, e3000435. [PubMed: 32168317]
39. Michael LF, Asahara H, Shulman AI, Kraus WL, and Montminy M (2000). The phosphorylation status of a cyclic AMP-responsive activator is modulated via a chromatin-dependent mechanism. Mol Cell Biol 20, 1596–1603. [PubMed: 10669737]
40. Hutchison AL, Maienschein-Cline M, Chiang AH, Tabei SM, Gudjonson H, Bahroos N, Allada R, and Dinner AR (2015). Improved statistical methods enable greater sensitivity in rhythm detection for genome-wide data. PLoS Comput Biol 11, e1004094. [PubMed: 25793520]
41. Bevacqua RJ, Lam JY, Peiris H, Whitener RL, Kim S, Gu X, Friedlander MSH, and Kim SK (2021). SIX2 and SIX3 coordinately regulate functional maturity and fate of human pancreatic beta cells. Genes Dev 35, 234–249. [PubMed: 33446570]
42. Reick M, Garcia JA, Dudley C, and McKnight SL (2001). NPAS2: an analog of clock operative in the mammalian forebrain. Science 293, 506–509. [PubMed: 11441147]
43. Wei G, Guo J, Doseff AI, Kusewitt DF, Man AK, Oshima RG, and Ostrowski MC (2004). Activated Ets2 is required for persistent inflammatory responses in the motheaten viable model. J Immunol 173, 1374–1379. [PubMed: 15240733]
44. Artner I, Hang Y, Mazur M, Yamamoto T, Guo M, Lindner J, Magnuson MA, and Stein R (2010). MafA and MafB regulate genes critical to beta-cells in a unique temporal manner. Diabetes 59, 2530–2539. [PubMed: 20627934]
45. Swisa A, Avrahami D, Eden N, Zhang J, Feleke E, Dahan T, Cohen-Tayar Y, Stolovich-Rain M, Kaestner KH, Glaser B, et al. (2017). PAX6 maintains beta cell identity by repressing genes of alternative islet cell types. J Clin Invest 127, 230–243. [PubMed: 27941241]

46. Remsberg JR, Ediger BN, Ho WY, Damle M, Li Z, Teng C, Lanzillotta C, Stoffers DA, and Lazar MA (2017). Deletion of histone deacetylase 3 in adult beta cells improves glucose tolerance via increased insulin secretion. Mol Metab 6, 30–37. [PubMed: 28123935]
47. Fujitani Y, Fujitani S, Boyer DF, Gannon M, Kawaguchi Y, Ray M, Shiota M, Stein RW, Magnuson MA, and Wright CV (2006). Targeted deletion of a cis-regulatory region reveals differential gene dosage requirements for Pdx1 in foregut organ differentiation and pancreas formation. Genes Dev 20, 253–266. [PubMed: 16418487]
48. Honma S, Kawamoto T, Takagi Y, Fujimoto K, Sato F, Noshiro M, Kato Y, and Honma K (2002). Dec1 and Dec2 are regulators of the mammalian molecular clock. Nature 419, 841–844. [PubMed: 12397359]
49. Zhao WN, Malinin N, Yang FC, Staknis D, Gekakis N, Maier B, Reischl S, Kramer A, and Weitz CJ (2007). CIPC is a mammalian circadian clock protein without invertebrate homologues. Nat Cell Biol 9, 268–275. [PubMed: 17310242]
50. Golombek DA, and Rosenstein RE (2010). Physiology of circadian entrainment. Physiol Rev 90, 1063–1102. [PubMed: 20664079]
51. Rakshit K, Qian J, Gaonkar KS, Dhawan S, Colwell CS, and Matveyenko AV (2018). Postnatal Ontogenesis of the Islet Circadian Clock Plays a Contributory Role in beta-Cell Maturation Process. Diabetes 67, 911–922. [PubMed: 29500314]
52. Stolovich-Rain M, Enk J, Vikesa J, Nielsen FC, Saada A, Glaser B, and Dor Y (2015). Weaning triggers a maturation step of pancreatic beta cells. Dev Cell 32, 535–545. [PubMed: 25662175]
53. Arda HE, Li L, Tsai J, Torre EA, Rosli Y, Peiris H, Spitale RC, Dai C, Gu X, Qu K, et al. (2016). Age-Dependent Pancreatic Gene Regulation Reveals Mechanisms Governing Human beta Cell Function. Cell Metab 23, 909–920. [PubMed: 27133132]
54. Gale JE, Cox HI, Qian J, Block GD, Colwell CS, and Matveyenko AV (2011). Disruption of circadian rhythms accelerates development of diabetes through pancreatic beta-cell loss and dysfunction. J Biol Rhythms 26, 423–433. [PubMed: 21921296]
55. Ou J, Liu H, Yu J, Kelliher MA, Castilla LH, Lawson ND, and Zhu LJ (2018). ATACseqQC: a Bioconductor package for post-alignment quality assessment of ATAC-seq data. BMC Genomics 19, 169. [PubMed: 29490630]
56. Anders S, and Huber W (2010). Differential expression analysis for sequence count data. Genome Biol 11, R106. [PubMed: 20979621]
57. Love MI, Huber W, and Anders S (2014). Moderated estimation of fold change and dispersion for RNA-seq data with DESeq2. Genome Biol 15, 550. [PubMed: 25516281]
58. Brown MR, Sen SK, Mazzone A, Her TK, Xiong Y, Lee JH, Javeed N, Colwell CS, Rakshit K, LeBrasseur NK, et al. (2021). Time-restricted feeding prevents deleterious metabolic effects of circadian disruption through epigenetic control of beta cell function. Sci Adv 7, eabg6856. [PubMed: 34910509]
59. Hong HK, Maury E, Ramsey KM, Perelis M, Marcheva B, Omura C, Kobayashi Y, Guttridge DC, Barish GD, and Bass J (2018). Requirement for NF-kappaB in maintenance of molecular and behavioral circadian rhythms in mice. Genes Dev 32, 1367–1379. [PubMed: 30366905]
60. Yang X, Graff SM, Heiser CN, Ho KH, Chen B, Simmons AJ, Southard-Smith AN, David G, Jacobson DA, Kaverina I, et al. (2020). Coregulator Sin3a Promotes Postnatal Murine beta-Cell Fitness by Regulating Genes in Ca(2+) Homeostasis, Cell Survival, Vesicle Biosynthesis, Glucose Metabolism, and Stress Response. Diabetes 69, 1219–1231. [PubMed: 32245798]
61. Ling L, and Goeddel DV (2000). MIP-T3, a novel protein linking tumor necrosis factor receptor-associated factor 3 to the microtubule network. J Biol Chem 275, 23852–23860. [PubMed: 10791955]
62. Boni-Schnetzler M, Boller S, Debray S, Bouzakri K, Meier DT, Prazak R, Kerr-Conte J, Pattou F, Ehses JA, Schuit FC, and Donath MY (2009). Free fatty acids induce a proinflammatory response in islets via the abundantly expressed interleukin-1 receptor I. Endocrinology 150, 5218–5229. [PubMed: 19819943]
63. Ramos-Rodriguez M, Raurell-Vila H, Colli ML, Alvelos MI, Subirana-Granes M, Juan-Mateu J, Norris R, Turatsinze JV, Nakayasu ES, Webb-Robertson BM, et al. (2019). The impact of

proinflammatory cytokines on the beta-cell regulatory landscape provides insights into the genetics of type 1 diabetes. Nat Genet 51, 1588–1595. [PubMed: 31676868]

64. Dinarello CA (2000). The role of the interleukin-1-receptor antagonist in blocking inflammation mediated by interleukin-1. N Engl J Med 343, 732–734. [PubMed: 10974140]
65. Timper K, Seelig E, Tsakiris DA, and Donath MY (2015). Safety, pharmacokinetics, and preliminary efficacy of a specific anti-IL-1alpha therapeutic antibody (MABp1) in patients with type 2 diabetes mellitus. J Diabetes Complications 29, 955–960. [PubMed: 26139558]
66. Wiedemann SJ, Trimigliozzi K, Dror E, Meier DT, Molina-Tijeras JA, Rachid L, Le Foll C, Magnan C, Schulze F, Stawiski M, et al. (2022). The cephalic phase of insulin release is modulated by IL-1beta. Cell Metab 34, 991–1003 e1006. [PubMed: 35750050]
67. Wang X, Sterr M, Burtscher I, Chen S, Hieronimus A, Machicao F, Staiger H, Haring HU, Lederer G, Meitinger T, et al. (2018). Genome-wide analysis of PDX1 target genes in human pancreatic progenitors. Mol Metab 9, 57–68. [PubMed: 29396371]
68. Ayala JE, Lantier L, McGuinness OP, and Wasserman DH (2022). Peeling back the layers of the glucose clamp. Nat Metab 4, 496–498. [PubMed: 35477775]
69. Weidemann BJ, and Bass J (2020). A window in time for beta-cell regeneration. Genes Dev 34, 1559–1561. [PubMed: 33262142]
70. Javeed N, Brown MR, Rakshit K, Her T, Sen SK, and Matveyenko AV (2021). Proinflammatory Cytokine Interleukin 1beta Disrupts beta-cell Circadian Clock Function and Regulation of Insulin Secretion. Endocrinology 162.
71. Nguyen HCB, Adlanmerini M, Hauck AK, and Lazar MA (2020). Dichotomous engagement of HDAC3 activity governs inflammatory responses. Nature 584, 286–290. [PubMed: 32760002]
72. Eckel-Mahan KL, Patel VR, de Mateo S, Orozco-Solis R, Ceglia NJ, Sahar S, Dilag-Penilla SA, Dyar KA, Baldi P, and Sassone-Corsi P (2013). Reprogramming of the circadian clock by nutritional challenge. Cell 155, 1464–1478. [PubMed: 24360271]
73. Sato S, Solanas G, Peixoto FO, Bee L, Symeonidi A, Schmidt MS, Brenner C, Masri S, Benitah SA, and Sassone-Corsi P (2017). Circadian Reprogramming in the Liver Identifies Metabolic Pathways of Aging. Cell 170, 664–677 e611. [PubMed: 28802039]
74. Norlin S, Ahlgren U, and Edlund H (2005). Nuclear factor-kappaB activity in beta-cells is required for glucose-stimulated insulin secretion. Diabetes 54, 125–132. [PubMed: 15616019]
75. Zammit NW, Wong YY, Walters SN, Warren J, Barry SC, and Grey ST (2023). RELA governs a network of islet-specific metabolic genes necessary for beta cell function. Diabetologia 66, 1516–1531. [PubMed: 37311878]
76. Turek FW, Joshu C, Kohsaka A, Lin E, Ivanova G, McDearmon E, Laposky A, Losee-Olson S, Easton A, Jensen DR, et al. (2005). Obesity and metabolic syndrome in circadian Clock mutant mice. Science 308, 1043–1045. [PubMed: 15845877]
77. Leproult R, Holmback U, and Van Cauter E (2014). Circadian misalignment augments markers of insulin resistance and inflammation, independently of sleep loss. Diabetes 63, 1860–1869. [PubMed: 24458353]
78. Hotamisligil GS (2006). Inflammation and metabolic disorders. Nature 444, 860–867. [PubMed: 17167474]
79. Maedler K, Sergeev P, Ris F, Oberholzer J, Joller-Jemelka HI, Spinas GA, Kaiser N, Halban PA, and Donath MY (2002). Glucose-induced beta cell production of IL-1beta contributes to glucotoxicity in human pancreatic islets. J Clin Invest 110, 851–860. [PubMed: 12235117]
80. Hajmrle C, Smith N, Spigelman AF, Dai X, Senior L, Bautista A, Ferdaoussi M, and MacDonald PE (2016). Interleukin-1 signaling contributes to acute islet compensation. JCI Insight 1, e86055. [PubMed: 27699257]
81. Marcheva B, Ramsey KM, Buhr ED, Kobayashi Y, Su H, Ko CH, Ivanova G, Omura C, Mo S, Vitaterna MH, et al. (2010). Disruption of the clock components CLOCK and BMAL1 leads to hypoinsulinaemia and diabetes. Nature 466, 571–572.
82. Yoo SH, Yamazaki S, Lowrey PL, Shimomura K, Ko CH, Buhr ED, Siepka SM, Hong HK, Oh WJ, Yoo OJ, et al. (2004). PERIOD2::LUCIFERASE real-time reporting of circadian dynamics reveals persistent circadian oscillations in mouse peripheral tissues. Proc Natl Acad Sci U S A 101, 5339–5346. [PubMed: 14963227]

83. Marcheva B, Perelis M, Weidemann BJ, Taguchi A, Lin H, Omura C, Kobayashi Y, Newman MV, Wyatt EJ, McNally EM, et al. (2020). A role for alternative splicing in circadian control of exocytosis and glucose homeostasis. Genes Dev 34, 1089–1105. [PubMed: 32616519]
84. Korsunsky I, Millard N, Fan J, Slowikowski K, Zhang F, Wei K, Baglaenko Y, Brenner M, Loh PR, and Raychaudhuri S (2019). Fast, sensitive and accurate integration of single-cell data with Harmony. Nat Methods 16, 1289–1296. [PubMed: 31740819]
85. Hao Y, Hao S, Andersen-Nissen E, Mauck WM 3rd, Zheng S, Butler A, Lee MJ, Wilk AJ, Darby C, Zager M, et al. (2021). Integrated analysis of multimodal single-cell data. Cell 184, 3573–3587 e3529. [PubMed: 34062119]
86. Gryder BE, Khan J, and Stanton BZ (2020). Measurement of differential chromatin interactions with absolute quantification of architecture (AQuA-HiChIP). Nat Protoc 15, 1209–1236. [PubMed: 32051612]
87. Servant N, Varoquaux N, Lajoie BR, Viara E, Chen CJ, Vert JP, Heard E, Dekker J, and Barillot E (2015). HiC-Pro: an optimized and flexible pipeline for Hi-C data processing. Genome Biol 16, 259. [PubMed: 26619908]
88. Lawrence M, Gentleman R, and Carey V (2009). rtracklayer: an R package for interfacing with genome browsers. Bioinformatics 25, 1841–1842. [PubMed: 19468054]
89. Bhattacharyya S, Chandra V, Vijayanand P, and Ay F (2019). Identification of significant chromatin contacts from HiChIP data by FitHiChIP. Nat Commun 10, 4221. [PubMed: 31530818]
90. Berglund ED, Li CY, Poffenberger G, Ayala JE, Fueger PT, Willis SE, Jewell MM, Powers AC, and Wasserman DH (2008). Glucose metabolism in vivo in four commonly used inbred mouse strains. Diabetes 57, 1790–1799. [PubMed: 18398139]
91. Ayala JE, Bracy DP, McGuinness OP, and Wasserman DH (2006). Considerations in the design of hyperinsulinemic-euglycemic clamps in the conscious mouse. Diabetes 55, 390–397. [PubMed: 16443772]
92. Buenrostro JD, Giresi PG, Zaba LC, Chang HY, and Greenleaf WJ (2013). Transposition of native chromatin for fast and sensitive epigenomic profiling of open chromatin, DNA-binding proteins and nucleosome position. Nat Methods 10, 1213–1218. [PubMed: 24097267]
93. Satija R, Farrell JA, Gennert D, Schier AF, and Regev A (2015). Spatial reconstruction of single-cell gene expression data. Nat Biotechnol 33, 495–502. [PubMed: 25867923]
94. Ulgen E, Ozisik O, and Sezerman OU (2019). pathfindR: An R Package for Comprehensive Identification of Enriched Pathways in Omics Data Through Active Subnetworks. Front Genet 10, 858. [PubMed: 31608109]
95. Yu G, Wang LG, and He QY (2015). ChIPseeker: an R/Bioconductor package for ChIP peak annotation, comparison and visualization. Bioinformatics 31, 2382–2383. [PubMed: 25765347]
96. Pliner HA, Packer JS, McFaline-Figueroa JL, Cusanovich DA, Daza RM, Aghamirzaie D, Srivatsan S, Qiu X, Jackson D, Minkina A, et al. (2018). Cicero Predicts cis-Regulatory DNA Interactions from Single-Cell Chromatin Accessibility Data. Mol Cell 71, 858–871 e858. [PubMed: 30078726]
97. Dobin A, Davis CA, Schlesinger F, Drenkow J, Zaleski C, Jha S, Batut P, Chaisson M, and Gingeras TR (2013). STAR: ultrafast universal RNA-seq aligner. Bioinformatics 29, 15–21. [PubMed: 23104886]
98. Li B, and Dewey CN (2011). RSEM: accurate transcript quantification from RNA-Seq data with or without a reference genome. BMC Bioinformatics 12, 323. [PubMed: 21816040]
99. Durand NC, Shamim MS, Machol I, Rao SS, Huntley MH, Lander ES, and Aiden EL (2016). Juicer Provides a One-Click System for Analyzing Loop-Resolution Hi-C Experiments. Cell Syst 3, 95–98. [PubMed: 27467249]
100. Ramirez F, Bhardwaj V, Arrigoni L, Lam KC, Gruning BA, Villaveces J, Habermann B, Akhtar A, and Manke T (2018). High-resolution TADs reveal DNA sequences underlying genome organization in flies. Nat Commun 9, 189. [PubMed: 29335486]

HIGHLIGHTS

- snATAC-seq reveals critical role of PDX1 gradient in adult human β-cell function
- PDX1-SIN3A co-repression of latent NF-κB enhancers determines β-cell identity
- Crosstalk between PDX1-BMAL1-NF-κB controls secretory and apoptotic gene networks
- Blocking peptide to IL-1β improves insulin secretion in PDX1 hypomorphic mice

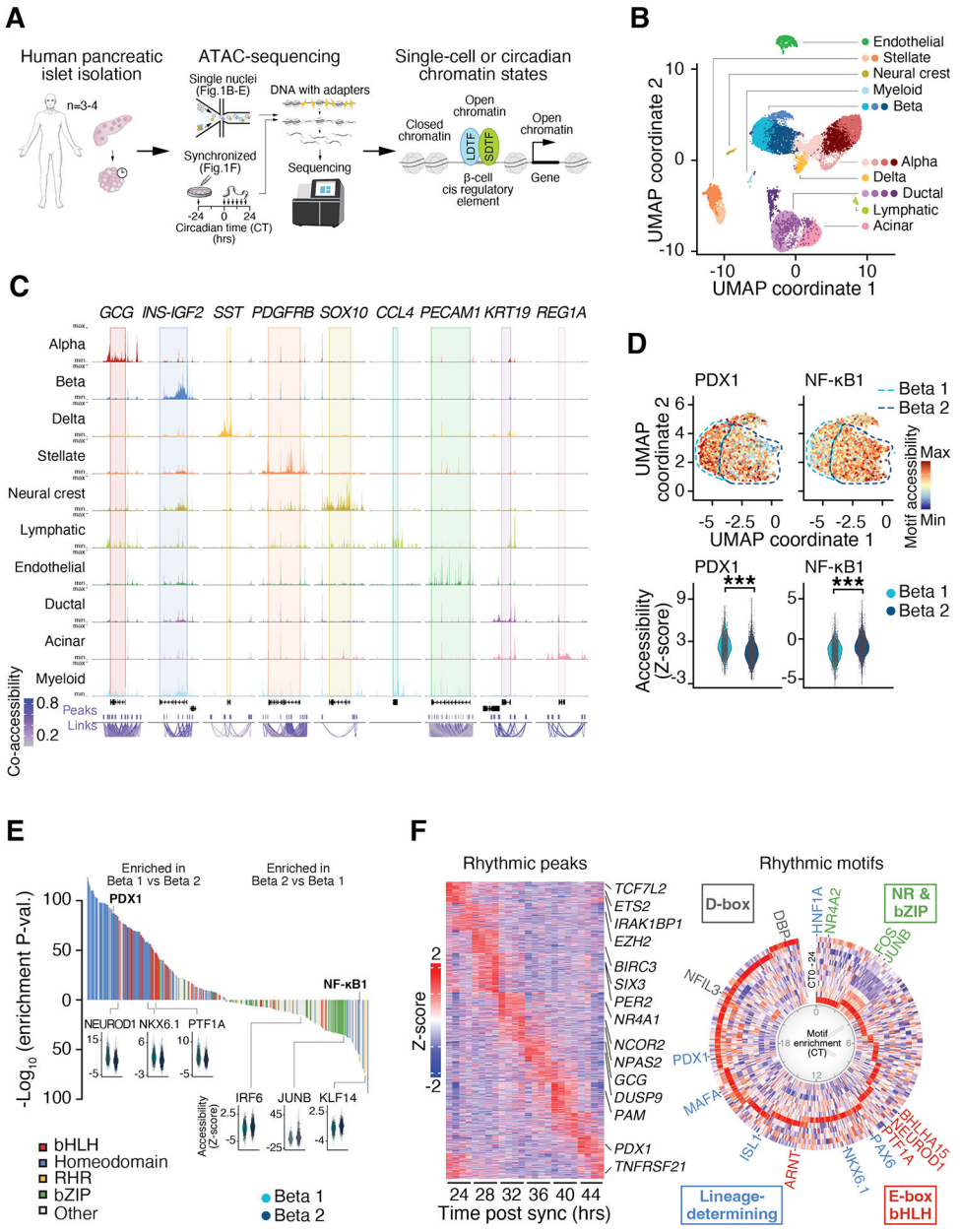

Figure 1. Single-cell chromatin accessibility sequencing identifies PDX1 and NF-κB enhancer signatures within distinct β-cell populations of the human islet.

(A) Profiling single nuclei and rhythmic bulk chromatin accessibility by ATAC-sequencing in human cadaveric islets. **(B)** Clustering and dimensional reduction analyses (UMAP) identified 19 distinct subpopulations of cells based on normalized reads at accessible cis-regulatory elements (20,519 single islet nuclei from 3 humans). **(C)** Aggregate sequencing fragments, segregated by cell-type, at lineage-specific marker genes: *GCG* (alpha), *INS-IGF2* (beta), *SST* (delta), *PDGFRB* (stellate), *SOX10* (neural crest), *CCL4* (lymphatic and myeloid immune), *PECAM1* (endothelial), *KRT19* (ductal), and *REG1A* (acinar). Co-accessibility linkage analysis connects individual snATAC-seq peak accessibility scores within networks of coregulated regions. **(D)** Accessibility at PDX1 (left) and NF-κB (right)

motifs was enriched in the β1 and β2 subpopulations of cells, respectively. Individual cell chromVAR z-scores (top) and subpopulation z-score distribution (bottom) across β1 and β2 subpopulations demonstrate significant variation in chromatin accessibility at PDX1 and NF-κB motifs. **(E)** Differential analysis of TF motif accessibility between β1 and β2 subpopulations revealed enrichment for basic helix-loop-helix (bHLH) and lineage-determining TFs in β1 cells and enrichment of immediate early bZIP and NF-κB TFs in β2 cells. **(F)** ATAC-seq performed in synchronized whole islets every 4 hrs for 24 hrs following a forskolin shock (n=10 human islet equivalents (IEQs) per sample per time point from 4 humans). Data was analyzed using eJTK_Cycle at a 2-hr resolution, revealing 24-hr patterns in chromatin opening at ATAC-seq peaks (left) and β-cell TF motifs associated with cell identity and rhythmic function (right). See also Figure S1 and Tables S1 and S3.

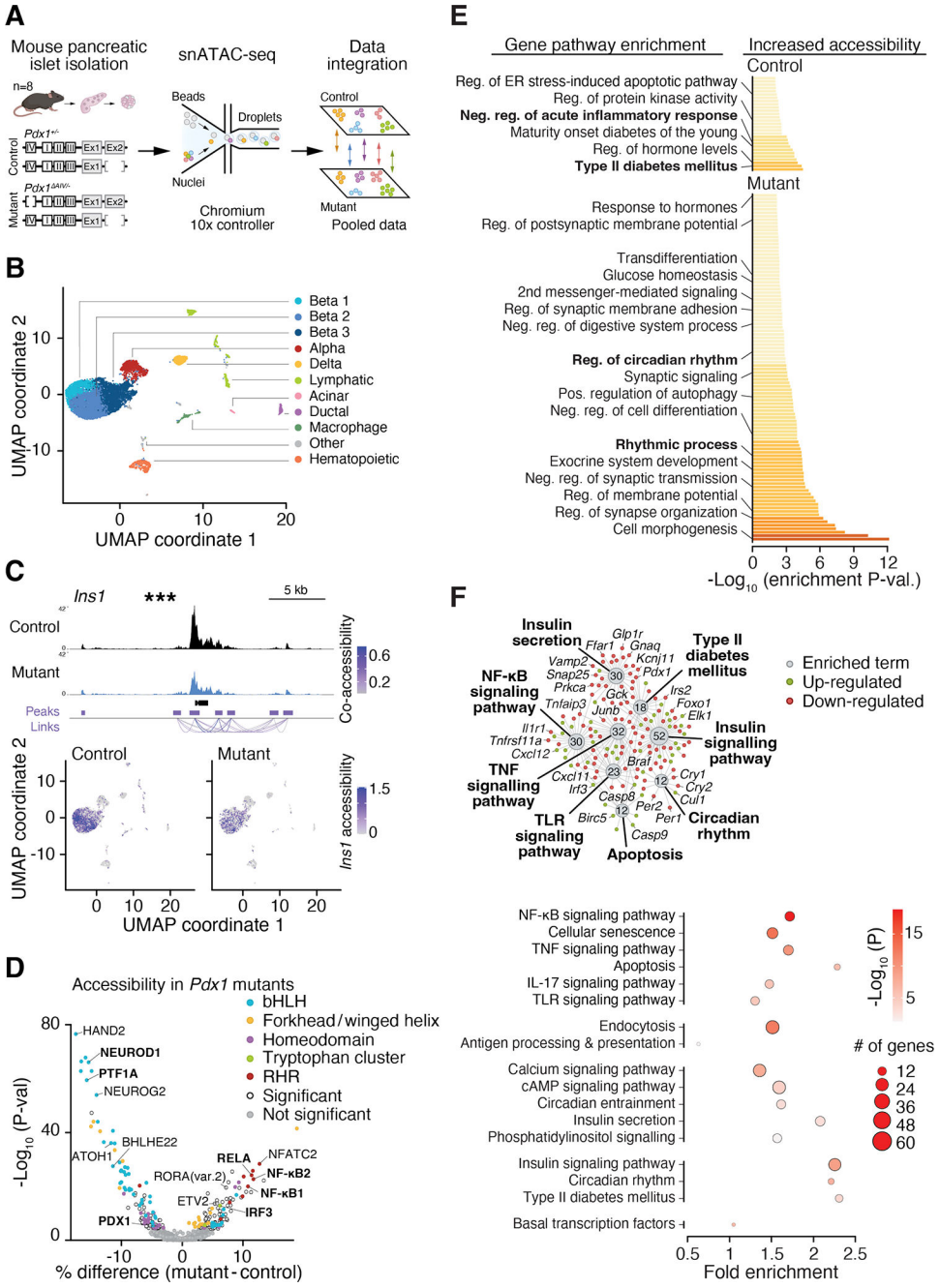

Figure 2. Genetic deficiency of PDX1 leads to de-repression of NF-κB.

(A) Profiling single-cell chromatin accessibility using single-nuclei ATAC-sequencing in islets isolated from control (*Pdx1*$^{+/-}$) and *Pdx1* mutant (*Pdx1*$^{\Delta AIV/-}$) mice (n=8 per genotype). **(B)** Clustering and dimensional reduction analyses (UMAP) of control and mutant islets cells identified 15 distinct subpopulations of cells based on normalized reads at accessible cis-regulatory elements. **(C)** Cumulative (top) and single-cell (bottom) accessible reads at the *Ins1* gene in pooled control versus *Pdx1* mutant β cells. **(D)** TF binding motifs differentially-enriched within accessible chromatin regions of pooled control versus *Pdx1* mutant β cells. Negative values indicate the motif is more enriched in controls, while

positive values indicate motif is more enriched in the *Pdx1* mutants. **(E)** Gene ontology analysis of annotated differentially-accessible peaks identified as upregulated in control or *Pdx1* mutant β cells. **(F)** RNA-sequencing reveals dysregulation of circadian, insulin secretion, and NF-κB signaling in *Pdx1A4* mutant islets. RNA-sequencing and pathway analyses using *pathfindR* reveal enrichment for circadian rhythm, insulin secretion, and NF-κB signaling KEGG pathways, as displayed by shared gene enrichment (top) and hierarchal clustering with fold-enrichment and multiple comparison P-values (bottom), among differentially-expressed transcripts (Adjusted P-value < 0.05) in islets isolated from *Pdx1A4* (n=5) versus *Pdx1* (n=4) heterozygous mice. See also Figure S2.

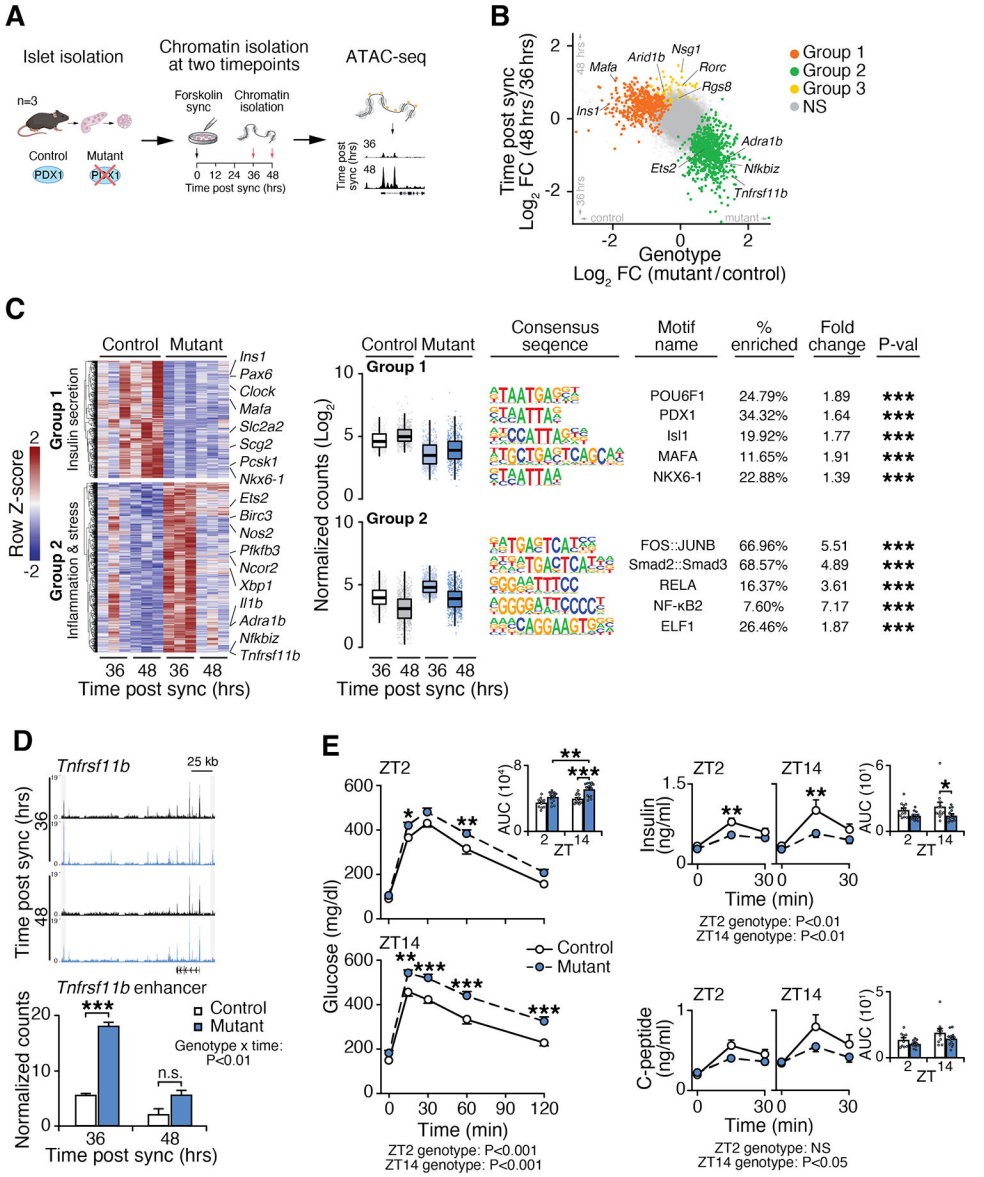

Figure 3. Circadian analyses reveal rhythmic regulation of NF-κB enhancer activity by PDX1.

(**A**) Pancreatic islet preparations from control (*Pdx1*$^{+/-}$) and *Pdx1* mutant (*Pdx1*$^{\Delta AIV/-}$) mice were subjected to a circadian synchronization pulse (forskolin), followed by ATAC-seq at two different time points, 36 and 48 hrs post-synchronization (the trough and peak of insulin secretion, respectively) (n=3 per timepoint per genotype). **(B)** Log2 fold-change in normalized accessible reads with respect to circadian time or genotype following identification of dynamic peaks using likelihood ratio tests. Significant peaks were segregated into different groups of peaks with distinct accessibility patterns using k-means clustering: Group 1 (orange) - sites with increased accessibility in control islets at the 48 hr time point (peak of insulin secretion) but with reduced accessibility in the mutants. Group 2 (green) - sites with increased accessibility at the 36 hr time point (trough of insulin secretion), which are also increased in the mutants. Group 3 sites (yellow) - sites only dependent on circadian time and not genotype. **(C)** Normalized accessible read Z-scores

(left, middle) across all samples reveal increased accessibility nearby insulin secretion genes in control islets (Group 1) and near stress and inflammatory genes in mutant islets (Group 2). Motif analyses (right) within differentially-accessible peaks demonstrate enrichment for β-cell TFs and inflammatory and immediate early TFs in Group 1 and Group 2 chromatin peaks, respectively. **(D)** Increased normalized chromatin reads in *Pdx1*$^{\Delta AIV/-}$ mutant islets neighboring the TNF-related gene *Tnfrsf11b* at 36 hrs post-synchronization. **(E)** Glucose clearance, insulin secretion, C-peptide levels, and area under curves following oral glucose administration (2g/kg) in control (n=14 mice per time point for glucose, n=13 for insulin and C-peptide) and *Pdx1* mutant (n=12 mice per time point for glucose, n=9 for insulin and C-peptide) in either the morning (ZT2) or evening (ZT14) analyzed by mixed-effects models. Main and interaction term significance determined by mixed-effects model. *P < 0.05, **P < 0.01, ***P < 0.001, n.s. not significant by Wald (ATAC-seq) or Holm-Šídák test. Data are represented as mean ± SEM. See also Figure S3.

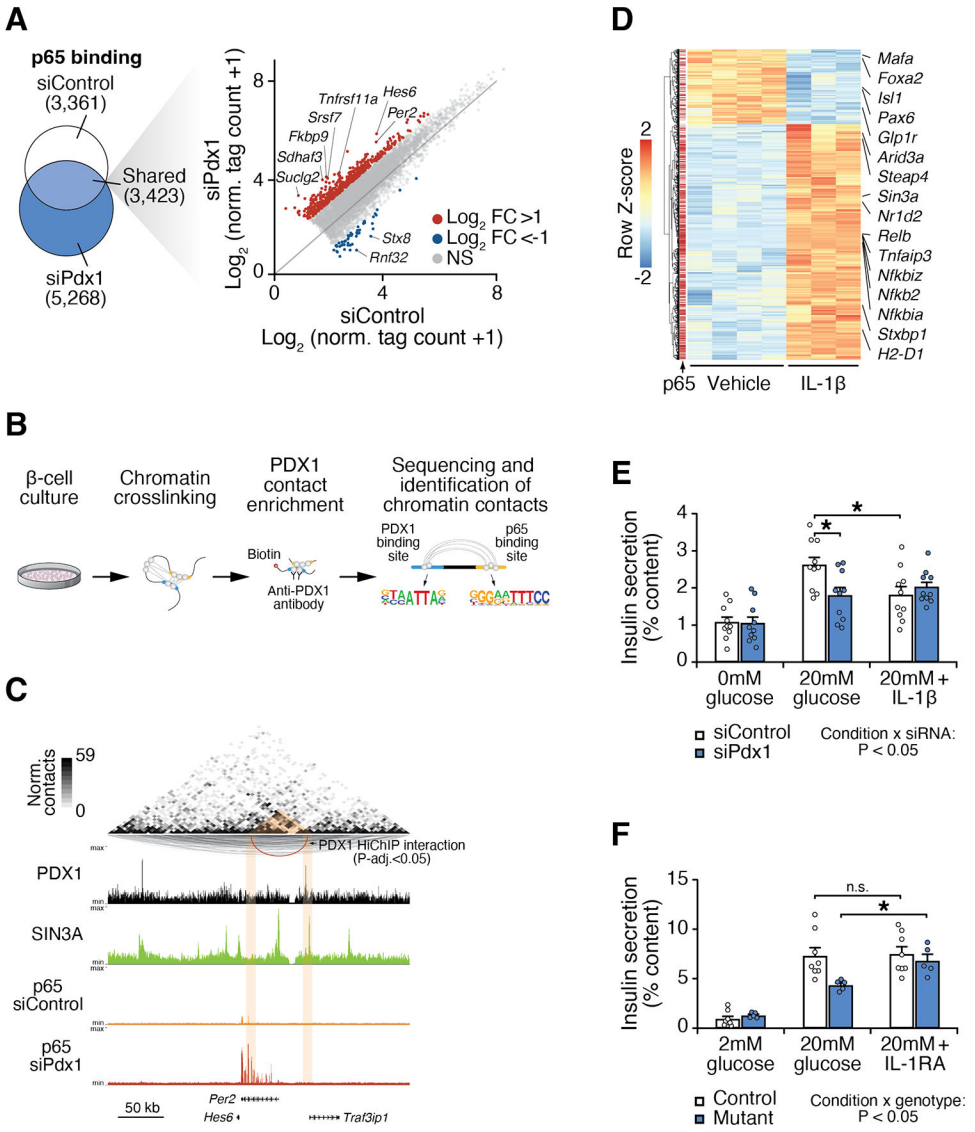

Figure 4. PDX1 represses NF-κB through long-range chromatin contacts that co-localize with IL-1β-response elements controlling insulin secretion.

(A) p65 ChIP-seq in Beta-TC-6 cells treated with siRNA targeting *Pdx1* (siPdx1) reveals increased genome-wide occupancy at inflammatory and circadian (*Per2*/*Hes6*) gene regions. **(B)** Chromatin conformational sequencing coupled with ChIP-seq (HiChIP-seq) targeting PDX1 identifies three-dimensional chromatin contacts involving PDX1 binding sites. **(C)** Significant chromatin interactions identified between the PDX1-SIN3A binding sites which loop to contact p65 binding sites. siPdx1-treated β cells exhibit increased p65 binding following loss of PDX1 protein, suggesting PDX1-SIN3A chromatin loops normally repress p65 binding near *Per2*. **(D)** IL-1β inhibits β-cell gene expression and activates p65-mediated expression of inflammatory genes in Beta-TC-6 cells. **(E)** Acute (2 hr) administration of IL-1β to β cells inhibits glucose-responsive insulin release specifically in control siRNA-treated cells, whereas siPdx1-treated cells do not respond to IL-1β (n=10 samples per siRNA treatment). Data are represented as mean ± SEM. **(F)** Antagonism of islet IL-1β signaling

using the IL-1β receptor antagonist (IL-1RA) restores glucose-stimulated insulin secretion in *Pdx1*$^{\Delta AIV/-}$ islets (n=8 *Pdx1*$^{+/-}$ mice, n=5 *Pdx1*$^{\Delta AIV/-}$ mice). Two-way ANOVA, *P < 0.05 by Holm-Šídák test. Data are represented as mean ± SEM. See also Figure S4 and Tables S4–S6.

Key Resources Table

REAGENT or RESOURCE	SOURCE	IDENTIFIER
Antibodies		
anti-p65	Cell Signaling	Cat#8242
anti-PDX1	Cell Signaling	Cat#5679
anti-BMAL1	J. Bass, Millipore	Cat#ABE2599
anti-SIN3A	Cell Signaling	Cat#8056S
anti-Histone H3	Cell Signaling	Cat#9715
anti-GAPDH	Cell Signaling	Cat#5174
HRP-linked anti-rabbit IgG	Cell Signaling	Cat#7074
RNAScope Reagents		
PDX1 RNAscope probe	ACD Bio	Cat#43081
INS1 RNAscope probe	ACD Bio	Cat#313571-C4
Human RNAscope 4-plex Positive Control Probes for RNAscope Multiplex Fluorescent Assay (*POLR2A*, *PPIB*, *UBC* and *HPRT1*	ACD Bio	Cat#321801
OPAL fluorophore 520	Akoya Biosciences	Cat#FP1487001KT
OPAL fluorophore 620	Akoya Biosciences	Cat#FP1495001KT
OPAL fluorophore 690	Akoya Biosciences	Cat#FP1497001KT
OPAL Polaris fluorophore 780	Akoya Biosciences	Cat#FP1501001KT
RNAscope 4-plex Multiplex Negative Control Probe	ACD Bio	Cat#321831
Bacterial and virus strains		
Biological samples		
Human islets	Integrated Islet Distribution Program (IIDP)	RRIDS: SAMN17928660, SAMN25519947, SAMN25980818, SAMN13134368, SAMN13254972, SAMN13515839, SAMN13739565, SAMN12227196, SAMN17928660, SAMN25519947
Chemicals, peptides, and recombinant proteins		
Forskolin	Sigma-Aldrich	Cat#F3917
Glucose	Sigma-Aldrich	Cat#G7528
Lipofectamine 3000	Thermo Fisher Scientific	Cat#L3000015
Recombinant IL-1B	Biolegend	Cat#575102
Recombinant mouse interleukin-1 receptor antagonist	Sigma-Aldrich	Cat#SRP6006
Recombinant human interleukin-1 receptor antagonist	MedChemExpress	Cat#AMG-719
TRI reagent	Molecular Research	Cat#NC9277980
Collagenase from *Clostridium histolyticum*	Sigma-Aldrich	Cat#C7657
Tagment DNA Enzyme (TE) and Buffer (TD)	Illumina	Cat#FC-121–1030
Formaldehyde	Polysciences	Cat#18814
Glycine	Fisher Scientific	Cat#BP381–5
DMSO	Sigma	Cat#D8418
Sodium chloride	Fischer Scientific	Cat#BP35–10

REAGENT or RESOURCE	SOURCE	IDENTIFIER
Ethylenediaminetetraacetic acid (EDTA)	Lonza	Cat#51234
NP-40	Sigma	Cat#NP40s
SDS	Sigma	Cat#L3771
Triton X-100	Sigma	Cat#X100
Trypsin	Fisher Scientific	Cat#25300054
Mini EDTA-free protease inhibitor cocktail	Roche	Cat#11836170001
HALT protease and phosphatase inhibitors	Thermo Fisher Scientific	Cat#78444
Anti-rabbit IgG dynabeads	Thermo Fisher Scientific	Cat#11204D
Streptavidin M280 dynabeads	Thermo Fisher Scientific	Cat#11205D
Penicillin-streptomycin	Gibco	Cat#15–140-122
L-glutamine	Fischer Scientific	Cat#25–030-081
Direct-zol miniprep columns	Zymo Research	Cat#R2052
NEBNext Poly(A) mRNA magnetic isolation module	New England Biolabs	Cat#E7490S
NEBNext Ultra II directional RNA library kit	New England Biolabs	Cat#E7760
NEBNext single cell/low input RNA library prep kit for Illumina	New England Biolabs	Cat#E6420S
Ampure XP reagent	Beckman	Cat#A63881
MinElute PCR purification kit	Qiagen	Cat#28004
Q5 High-Fidelity 2X master mix	New England Biolabs	Cat#M0492L
Di(N-succinimidyl) glutarate (DSG)	Proteochem	Cat#C1104
Biocoll	Millipore	Cat#L6155
Critical commercial assays		
Insulin ELISA Assays	Crystal Chem Inc	Cat#90082
C-peptide ELISA Assays	Crystal Chem Inc	Cat#90050
NextSeq 500/550 High Output Kit v2.5 (75 Cycles)	Illumina	Cat#20024906
NextSeq 2000 P3 Reagents (100 Cycles)	Illumina	Cat#20040559
NE-PER Nuclear and Cytoplasmic Reagent Kit	Thermo Fisher Scientific	Cat#78835
Deposited data		
Sequence data, analyses, and resources related to the sequencing of human and mouse tissues and cells	Gene Expression Omnibus	GSE214678
Experimental models: Cell lines		
Beta-TC-6 cells	American Type Culture Collection (ATCC)	CRL-11506
BMAL1 KO cells	Dr. Joseph Bass, Northwestern University	
Experimental models: Organisms/strains		
Pdx1$^{+/-}$ mice	Dr. Roland Stein, Vanderbilt University	
Pdx1$^{\Delta AIV/-}$ mice	Dr. Roland Stein, Vanderbilt University	
Per^{Luc} mice	Dr. Joseph Takahashi, UT Southwestern	
Oligonucleotides		

REAGENT or RESOURCE	SOURCE	IDENTIFIER
Anti-Pdx1 siRNA	ThermoFisher	Cat#4390771
Select Negative Control No. 1 siRNA	ThermoFisher	Cat#AM4611
ATAC-seq indexing primers 1–12 [92]	Integrated DNA Technologies	Custom order
Recombinant DNA		
Software and algorithms		
R (v4.1.2)	The R Foundation	
DESeq2 package (v1.36.0)	Love, 2014[57]	Bioconductor
Seurat package (v4.1.0)	Satija, 2015[93]	Bioconductor
pathfindR (v2.3.0)	Ulgen[94]	
Lme package (v1.1)	DOI: 10.18637/jss.v067.i01	Bioconductor
Cell Ranger ATAC (v2.0.0)	10X Genomics	https://www.10xgenomics.com/software
Cell Ranger (v6.1.2)	10X Genomics	https://www.10xgenomics.com/software
ChIPseeker package (v1.31.3)	Yu, 2015[95]	Bioconductor
ChromVAR package (v1.16.0)	Schep, 2017[27]	Bioconductor
Cicero package (v1.3.5)	Pliner, 2018[96]	Bioconductor
STAR (v2.5.0)	Dobin, 2013[97]	https://github.com/alexdobin/STAR
RSEM (v1.3.3)	Li, 2011[98]	https://github.com/deweylab/RSEM
Prism (v9.0)	GraphPad	
HiC-Pro (v3.1.0)	Servant 201[87]	https://github.com/nservant/HiC-Pro
Juicer (v1.6)	Durand, 20 1 6[99]	https://github.com/aidenlab/juicer
HiC-Explorer (v2.2)	Ramirez, 2018[100]	https://github.com/deeptools/HiCExplorer
FitHiChIP (v8.0)	Bhattacharyya, 2019[89]	https://github.com/ay-lab/FitHiChIP
ClockLab Data Collection and Analysis System (v6.0)	Actimetrics	https://actimetrics.com
Other		
Islet snATAC-seq dataset	Chiou, 2021[3]	GSE160472, GSE160473, GSE163610
Islet snRNA-seq dataset	Xin, 2018[25]	GSE114297
R scripts and objects		https://github.com/bjw032/PDX1_scATAC